

JGR Solid Earth

RESEARCH ARTICLE

10.1029/2022JB026269

Re-Examining Temporal Variations in Intermediate-Depth Seismicity

Sam Wimpenny¹ , Tim Craig¹ , and Savvas Marcou^{1,2} 

¹School of Earth and Environment, COMET, Institute for Geophysics and Tectonics, University of Leeds, Leeds, UK, ²Now at Berkeley Seismological Laboratory, University of California, Berkeley, Berkeley, CA, USA

Key Points:

- Large intraslab and megathrust earthquakes have a limited influence on the frequency of intermediate-depth seismicity
- Faults within subducted slabs are relatively insensitive to static stress transfer caused by earthquake stress drops
- Low stress drops and heterogeneous aftershock productivity can be best explained by dehydration-related weakening mechanisms

Supporting Information:

Supporting Information may be found in the online version of this article.

Correspondence to:

S. Wimpenny,
earswi@leeds.ac.uk

Citation:

Wimpenny, S., Craig, T., & Marcou, S. (2023). Re-examining temporal variations in intermediate-depth seismicity. *Journal of Geophysical Research: Solid Earth*, 128, e2022JB026269. <https://doi.org/10.1029/2022JB026269>

Received 15 DEC 2022

Accepted 1 JUN 2023

Author Contributions:

Conceptualization: Sam Wimpenny, Tim Craig, Savvas Marcou

Formal analysis: Sam Wimpenny, Tim Craig, Savvas Marcou

Funding acquisition: Tim Craig

Methodology: Sam Wimpenny, Tim Craig, Savvas Marcou

Writing – original draft: Sam Wimpenny

Writing – review & editing: Tim Craig, Savvas Marcou

© 2023. The Authors.

This is an open access article under the terms of the [Creative Commons Attribution License](https://creativecommons.org/licenses/by/4.0/), which permits use, distribution and reproduction in any medium, provided the original work is properly cited.

Abstract Changes in the frequency of intermediate-depth (60–300 km) earthquakes in response to static stress transfer can provide insights into the mechanisms of earthquake generation within subducting slabs. In this study, we use the most up-to-date global and regional earthquake catalogs to show that both the aftershock productivity of large earthquakes, and the changes in the frequency of intermediate-depth earthquakes around the timing of major megathrust slip, support the view that faults within the slab are relatively insensitive to static stress transfer on the order of earthquake stress drops. We interpret these results to suggest the population of faults within the slab are much further from their failure stress than is typical for shallow fault systems. We also find that aftershock productivity varies within slabs over small spatial scales, indicating that the mechanism that enables faults to rupture at intermediate depths is likely to be spatially heterogeneous over length-scales of a few tens of kilometres. We suggest dehydration-related weakening mechanisms can best account for this heterogeneity.

Plain Language Summary Earthquakes at 60–300 km depth within subducting slabs are known as “intermediate-depth” earthquakes. At such depths, the high pressures should act to clamp faults shut, preventing them from breaking in earthquakes through frictional sliding. In this study, we investigate the mechanisms that enable the generation of intermediate-depth earthquakes by examining the temporal changes of intermediate-depth seismicity caused by other, nearby earthquakes. We find that seismicity within slabs is relatively insensitive to the stress changes caused by nearby earthquakes when compared to shallow earthquakes of equivalent size. We interpret these results to suggest that faults within the slab are much further from their failure stress than is typical for shallow faults, and that the mechanism that enables faults to rupture at intermediate depth is likely to be spatially variable over length-scales of a few tens of kilometres. We suggest weakening mechanisms related to water release within slabs can best account for this heterogeneity.

1. Introduction

Temporal variations in the frequency of intermediate-depth (60–300 km) earthquakes have the potential to provide insights into the enigmatic conditions and mechanism(s) of earthquake nucleation within subducting slabs. These intraslab earthquakes have dominantly double-couple focal mechanisms, indicating they represent shear failure on a population of faults (Frohlich, 1989). However, at depths ≥ 60 km, the high confining pressures and high temperatures should prevent frictional failure on faults subject to normal plate-driving forces without an additional mechanism that reduces the stress needed to generate earthquake rupture (Zhan, 2020).

Two main mechanisms have been proposed: dehydration-related weakening and self-localizing thermal runaway. Dehydration-related weakening is caused by the breakdown of hydrous mafic minerals as the slab subducts, which either releases water that reduces the effective frictional strength of intraslab faults (dehydration embrittlement; Green & Houston, 1995; Hacker et al., 2003), or causes extreme stress concentrations through the breakdown of load-bearing hydrous phases (dehydration-assisted stress transfer; Ferrand et al., 2017), allowing faults to fail through frictional sliding. Alternatively, self-localizing thermal runaway is a process by which creep in hydrated or fine-grained shear zones causes shear heating and the development of ductile instabilities that relax elastic strain (Hobbs & Ord, 1988; Ogawa, 1987). Thermal runaway may have a nucleation phase involving progressive ductile strain, eventually leading up to seismogenic failure that relaxes the majority of the stored elastic strain in high stress-drop events (500–1,000 MPa; John et al., 2009; Kelemen & Hirth, 2007). These different mechanisms can account for the observation of earthquake generation at high confining pressures, but they should be

sensitive to different physical and mechanical conditions within the slab, such as temperature and the availability of hydrous mineral phases.

Progress in our understanding of intermediate-depth earthquake generation has therefore focused on explaining the spatial pattern of seismicity within subduction zones, such as the structure of double-seismic zones (e.g., Florez & Prieto, 2019; Sippl et al., 2019; Wei et al., 2017), or the relationship between intermediate-depth earthquake focal mechanisms, seismicity rates, and the orientation and density of outer-rise normal faulting (e.g., Boneh et al., 2019; Warren et al., 2007). Analysis of any temporal variations in the frequency of intermediate-depth seismicity can potentially provide complementary information to these studies. In particular, variations in the frequency of seismicity in response to known stress changes can provide insights into the population of faults that are close to failure, as well as the sensitivity of the failure mechanism to small stress perturbations, and how these vary between different pressure-temperature conditions and slab environments (e.g., Bouchon et al., 2016, 2018; Luo & Wiens, 2020; Persh & Houston, 2004; Tibi et al., 2003; Zhan & Shearer, 2015).

Two observations have emerged that suggest different sensitivities of intraslab faults systems to changes in static stress. First, studies have reported changes in the frequency of intraslab intermediate-depth earthquakes related to the occurrence of shallow earthquakes, including: (a) year-long changes in earthquake frequency that begin after large, shallow earthquakes on the adjacent subduction megathrust (Bouchon et al., 2016; Jara et al., 2017; Lay et al., 1989; Mitsui et al., 2021), and (b) month-long transient changes in intraslab earthquake frequency following slip on the megathrust (Delbridge et al., 2017). These observations suggest that intraslab faults in some settings are relatively sensitive to the small (<1 MPa) stress changes that shallow earthquakes impose on the slab through static stress transfer, and that faults within the subduction system are interacting with one another over distances of tens to hundreds of kilometres. In contrast, intermediate-depth earthquakes are consistently followed by far fewer aftershocks compared to shallow crustal earthquakes of equivalent magnitude (low “after-shock productivity”) (Frohlich, 1987; Persh & Houston, 2004; Wiens & Gilbert, 1996; Ye et al., 2020). As the stress drops in intermediate-depth earthquakes are similar to shallow earthquakes (~1–50 MPa) (Allmann & Shearer, 2009; Poli & Prieto, 2016; Tian et al., 2022), the difference in aftershock productivity between shallow and intermediate-depth mainshocks is not related to the amplitude of the stress changes. Rather, the low productivity of intermediate-depth aftershock sequences indicates that the faults within the slab are relatively insensitive to the stress changes caused by nearby large earthquakes within the slab, and that they only weakly interact with one another. These two inferences relating to intraslab seismicity appear to be in contradiction. This study aims to reconcile them by re-examining the evidence for temporal changes in the frequency of intermediate-depth seismicity around the timing of large earthquakes using the most up-to-date global and regional earthquake catalogues.

Section 2 focuses on the aftershock sequences of large intermediate-depth earthquakes, verifying previous results regarding their low aftershock productivity and testing whether aftershock productivity varies systematically with source or slab setting. Section 3 then explores the response of intermediate-depth seismicity to slip in megathrust earthquakes. We find that, although there are temporal variations in the frequency of intermediate-depth seismicity, they do not consistently correlate with the timing of stress changes caused by large megathrust earthquakes. In Section 4, we discuss the implications of our findings for the mechanics of faulting at intermediate depths within slabs.

2. Aftershock Productivity of Intermediate-Depth Earthquakes

Aftershocks are the most obvious manifestation of changes in seismicity rates, and reflect the rupture of faults in response to changes in the local stress state following a larger earthquake (King et al., 1994; Lin & Stein, 2004). Analyses of aftershock sequences following intermediate-depth earthquakes show that they are typically less productive compared to shallow earthquakes of equivalent magnitude (Dascher-Cousineau et al., 2020; Frohlich, 1987; Wiens & Gilbert, 1996; Ye et al., 2020). Aftershock productivity is also known to be depth-dependent, with most large earthquakes between 300 and 500 km often having no aftershocks at all with $m_b \geq 4.5$ (Persh & Houston, 2004). Early studies suggested that the aftershock productivity correlates with a slab's thermal structure (Wiens & Gilbert, 1996), though more recent work using longer-duration catalogs with lower magnitudes of completeness has argued that aftershock productivity is independent of slab temperature, but may be related to the heterogeneity of the stress field and fault network surrounding the mainshock (Ye et al., 2020) or the availability of highly pressurized free fluid in the slab (Cabrera et al., 2021; Chu & Beroza, 2022).

Below, we re-examine aftershock productivity at both global and regional scales using modern earthquake catalogues, focusing particularly on seismicity within the depth range 60–300 km. In this depth range, earthquakes are mostly within subducted oceanic lithosphere. Through this updated analysis, we aim to characterise the relative sensitivity of fault systems to earthquake stress changes in different slab environments by first focusing on global patterns in aftershock productivity and then zooming in to region-scale patterns.

2.1. Global Analysis

2.1.1. Method of Measuring Aftershock Productivity

We first studied the aftershock sequences of all $M_w > 6.5$ earthquakes using a simple clustering algorithm applied to the ISC's reviewed global catalog following the methods of Baiesi and Paczuski (2004) and Zaliapin and Ben-Zion (2013). We use this non-parametric clustering method, as it does not assume any particular form for the temporal evolution of aftershock frequency (e.g., Chu & Beroza, 2022; Dascher-Cousineau et al., 2020). The ISC's reviewed earthquake catalog is derived from a location procedure that uses the body-wave phase arrivals from teleseismic and regional stations to provide the most accurate estimates of earthquake hypocentral parameters and consistent body-wave magnitude estimates globally (Bondár & Storchak, 2011; Di Giacomo & Storchak, 2016). We complement these data with moment tensor information for each mainshock derived using long-period body and surface wave inversion from the global Centroid Moment Tensor (gCMT) catalog (Dziewonski et al., 1981; Ekström et al., 2012), which limits the time-span of our analysis to mainshocks between 1976 and 2020. We choose to represent the size of the mainshocks using the moment magnitude M_w derived by the gCMT, and not body-wave magnitude m_b , because the body-wave magnitude scale saturates for the largest mainshocks included in our analysis at $m_b \gtrsim 7.5$.

For each mainshock, we began by taking a subset of events from the ISC catalog that are within 500 km of the mainshock hypocenter and which have $m_b \geq 4.5$. For all events within this subset, we then calculated the space-time distance η_{ij} between each event hypocenter i and every other event hypocenter j (Zaliapin et al., 2008). The space-time distance is defined as $\eta_{ij} = t_{ij}(r_{ij})^d 10^{-bm_i}$, where $t_{ij} = t_j - t_i$ is the time difference between event origin times, r_{ij} is the 3-dimensional cartesian distance between the event hypocenters, m_i is the magnitude of event i , and $d = 1.6$ and $b = 1$ are constants (Zaliapin & Ben-Zion, 2013). If $t_{ij} \leq 0$ then we set $\eta_{ij} = \infty$ to enforce causality (i.e., event j must have occurred after event i for it to be an aftershock). The choice of $m_b \geq 4.5$ is designed to capture a global average for the magnitude of completeness for intermediate-depth seismicity (Ye et al., 2020). Although changing this value to $m_b \geq 5.0$ has an effect on the absolute count of aftershocks, it has little effect on the trends in relative aftershock productivity (Text S1 in Supporting Information S1).

For every event j in the catalog we define its parent as the event i for which $\eta_j = \min(\eta_{ij})$. At this stage we check that the mainshock is not an aftershock of an even larger earthquake by ensuring that, for the event to be considered a mainshock, it has no parent events that have a larger magnitude. The resulting distribution of $\log_{10}(\eta_j)$ forms two peaks (Figure S1a in Supporting Information S1), with events with low $\log_{10}(\eta_j)$ being clustered events and those with high $\log_{10}(\eta_j)$ being independent events (Zaliapin & Ben-Zion, 2013). To determine the cut-off between the two, we fit a two-component Gaussian mixture model to the distribution and determined the overlap between the two curves η_0 (Figure S1b in Supporting Information S1). We then recursively counted all of the offspring of the mainshock that have $\eta_j \leq \eta_0$ to yield the final aftershock count. The seismicity that is not clustered, which consists of all events for which $\eta_j > \eta_0$, is used to calculate the background seismicity rate within ± 50 km horizontal distance and ± 30 km depth around each mainshock (Figure S2 in Supporting Information S1).

The analysis described above yields aftershock counts for 2,432 mainshocks. For the remaining 1586 events with $M_w \geq 6.5$ in the gCMT catalog, we were either not able to separate the background from the clustered seismicity, or the earthquake was itself an aftershock. Although the absolute aftershock count is weakly dependent on the constants used in the space-time distance calculation (b , d , and η_0), the relative count between mainshocks is insensitive to the parameter selection (Text S1 in Supporting Information S1). Below we only interpret changes in relative aftershock productivity.

2.1.2. Results of Aftershock Productivity Analysis

Figure 1 shows the number of aftershocks for each mainshock plotted against a set of possible dependent variables. The two clear trends within the data are that the aftershock productivity changes as a function of mainshock

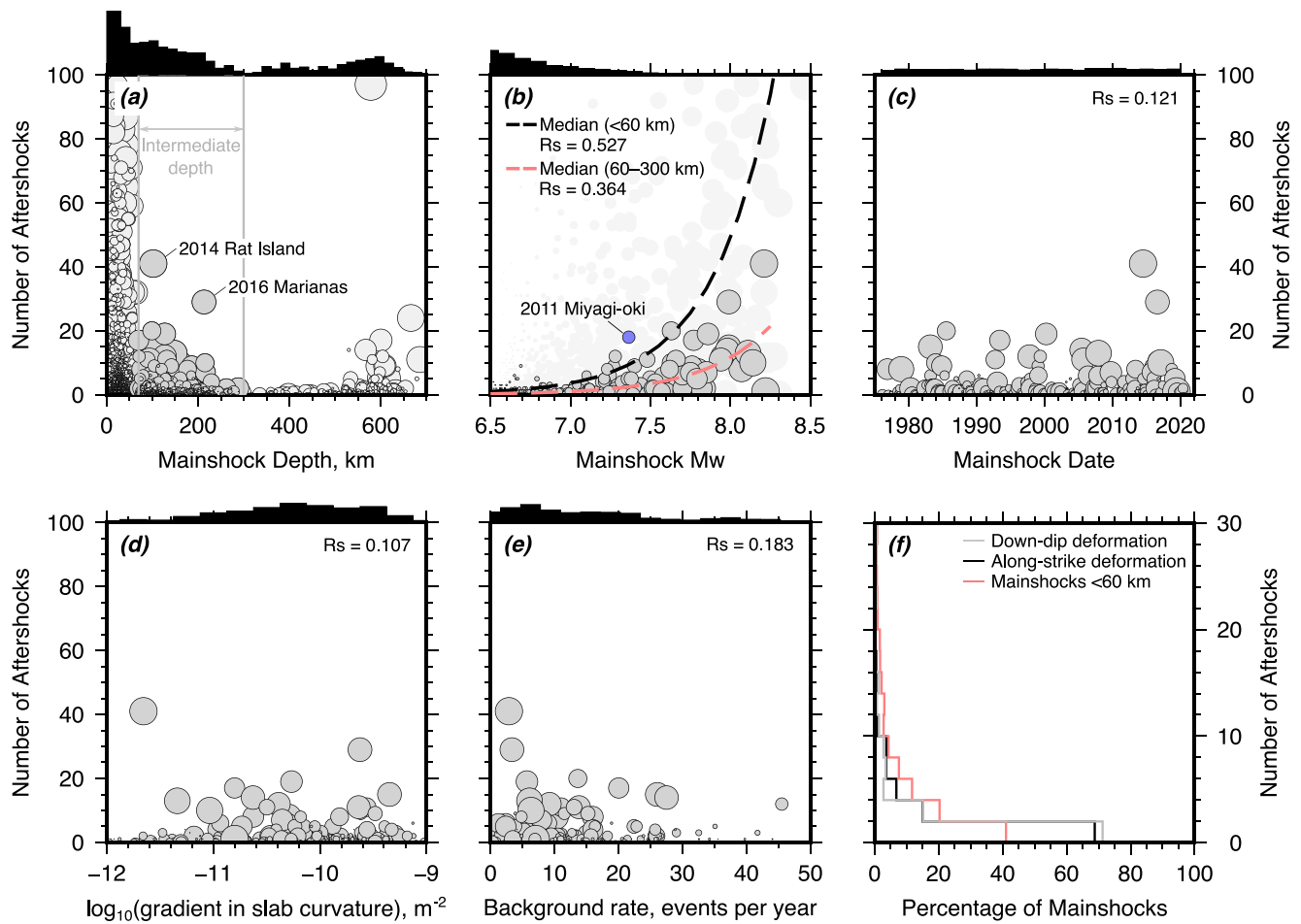


Figure 1. Aftershock productivity for earthquakes in the gCMT catalog with $M_w \geq 6.5$. (a) Aftershock productivity as a function of the mainshock depth. Intermediate-depth earthquakes (60–300 km) are shown in dark gray. The histogram of the logarithm of mainshock frequency with depth is shown above. (b) Aftershock productivity as a function of mainshock magnitude. Intermediate-depth earthquakes are shown in dark gray with black outline, whilst earthquakes with hypocentral depths <60 km are shown as light gray circles. The median aftershock productivity scaling is shown for shallow and intermediate-depth mainshocks. R_s is the Spearman's Correlation Coefficient. (c) Aftershock productivity as a function of mainshock date, (d) the gradient in the down-dip curvature of the slab at the centroid location computed from Slab 2.0 (Hayes et al., 2018), and (e) the background seismicity rate within 50 km horizontal distance and ± 30 km depth difference from the mainshock hypocenter. (f) Histogram of aftershock productivity for mainshocks that accommodate either along-strike or down-dip deformation of the slab. The red histogram shows the productivity for shallow earthquakes with hypocentral depths <60 km.

depth and mainshock magnitude (Figures 1a and 1b) (Frohlich, 1987; Persh & Houston, 2004; Ye et al., 2020). In terms of mainshock depth, we find that there is a sharp decrease in aftershock productivity as mainshocks exceed 50–60 km depth (Figure 1a), which roughly corresponds to the transition from shallow crustal and intraplate seismicity to intraslab seismicity. Below 60 km depth, the median aftershock productivity continues to decrease with depth until 300 km, then remains consistently low for mainshocks between 300 and 500 km depth, before increasing again between 500 and 700 km depth, mirroring the distribution of mainshocks (Figure 1a).

Aftershock productivity also increases with mainshock magnitude (Figure 1b). For earthquakes within both the shallow (<60 km) and intermediate-depth range (60–300 km), the median aftershock productivity scaling with mainshock magnitude M can be fit by an equation of the form $a10^{\gamma(M-M_c)}$ where $\gamma \approx 1$ and M_c is the magnitude of completeness (Frohlich, 1987) (Figure S5 in Supporting Information S1). The median aftershock productivity for the intermediate depth earthquakes consistently falls below that for shallow earthquakes across the mainshock magnitude range (Figure 1b), indicating that intermediate-depth earthquakes have, at least on average, fewer aftershocks for a given magnitude mainshock. However, there is still significant scatter in aftershock productivity around the median for intermediate-depth earthquakes. The scatter indicates there is some other control on the measured aftershock productivity beyond just mainshock depth and magnitude.

One possibility is that the scatter is related to our method of aftershock counting. We found no correlation between the aftershock productivity and the date of the mainshock, suggesting temporal changes in the ISC catalog's completeness are not contributing to the scatter (Figure 1c). In addition, the aftershock productivity does not correlate with the gradient in down-dip slab curvature or background seismicity rate (Figures 1d and 1e), which implies that aliasing high rates of background seismicity into aftershock productivity is also not contributing to the scatter.

Alternatively, the scatter in aftershock productivity may relate to an unidentified mechanism associated with the mainshock source or setting, such as the mechanical properties of the slab (Wiens & Gilbert, 1996) or stress heterogeneity and variability in fault geometries within the slab (Ye et al., 2020). For almost every mainshock the aftershocks of large intermediate-depth earthquakes are too small to have mechanisms in the gCMT catalog, limiting our ability to test whether aftershock productivity is related to the geometry of the receiver faults. However, if aftershock productivity were related to the slab setting, then it should vary systematically between subduction zones.

After removing the scaling between the median aftershock productivity and mainshock magnitude, we did not find any systematic spatial variability in aftershock productivity at the scale of individual subduction zones (Text S2 in Supporting Information S1). However, this analysis is limited by there being too few $M_w \geq 7.5$ events to identify any spatially robust trends, and earthquakes in the magnitude range $6.5 \leq M_w < 7.5$ have too few aftershocks (generally < 5 ; see Figure 1b) of $m_b \geq 4.5$ to record spatial variability in the aftershock productivity using global catalogs (Text S2 in Supporting Information S1).

Earthquakes on transform faults produce the fewest aftershocks of any shallow fault zones (Boettcher & Jordan, 2004; Dascher-Cousineau et al., 2020). Therefore, we also examined whether aftershock productivity is controlled by the geometry of pre-existing faults present in subducted oceanic lithosphere, particularly whether intermediate-depth earthquakes may be reactivating outer-rise faults or fracture zones. As outer-rise faults form parallel to the trench and perpendicular to the slab dip direction, we first tested whether aftershock productivity depends on whether the mainshock accommodates down-dip or along-strike deformation of the slab based on the mainshock's P and T axes. We found that, irrespective of whether the mainshock accommodates down-dip or along-strike deformation, the two populations of intermediate-depth events have similar aftershock productivity statistics (Figure 1f). Identifying where intermediate-depth earthquakes may be reactivating fracture zones is more difficult, because of the ambiguity in which nodal plane is the rupture plane. However, we note that areas where the fracture zones are almost perpendicular to the trench, such as in South America, the intermediate-depth earthquakes accommodate down-dip extension of the slab and are not reactivating fracture zones, but still have low aftershock productivity for their magnitude (Text S2 in Supporting Information S1).

Therefore, features unique to a particular slab, at least at the scale of hundreds of kilometres resolvable with global catalog data, seem unable to explain the scatter in aftershock productivity between events of similar magnitude. In the next section, we test whether higher-resolution regional earthquake catalogs with lower magnitudes of completeness can provide insights into the controls on intermediate-depth aftershock productivity not resolvable using the global seismic catalog.

2.2. Regional Analysis: Northern Chile

High-resolution regional earthquake catalogs can provide better constraints on the spatial variability in aftershock productivity and its relationships with the mainshock setting (Chu & Beroza, 2022; Gomberg & Bodin, 2021; Sippl et al., 2019). We re-assessed the aftershock productivity of moderate-magnitude earthquakes in northern Chile, because this region has: (a) an earthquake catalog that contains over 100,000 earthquakes of $M_L \geq 2.0$ from 2006 to 2015 (Sippl et al., 2018), (b) a highly seismogenic slab at intermediate depths, and (c) relatively consistent earthquake mechanisms and magnitudes that allows for comparison between events with a similar source.

We applied the same aftershock identification algorithm to the catalog of Sippl et al. (2018) for all earthquakes with $M_w \geq 5.3$ that have moment tensors in the gCMT catalog and include all events above the completeness $M_L \geq 2.8$ as possible aftershocks (Figure 2). This analysis leads to aftershock counts for 22 shallow mainshocks (< 60 km depth) and 92 intermediate-depth mainshocks (60–300 km depth). There is not enough diversity amongst the magnitudes of these large mainshocks to robustly calculate a scaling between mainshock magnitude and aftershock productivity, which limits our ability to compare the relative aftershock productivity of

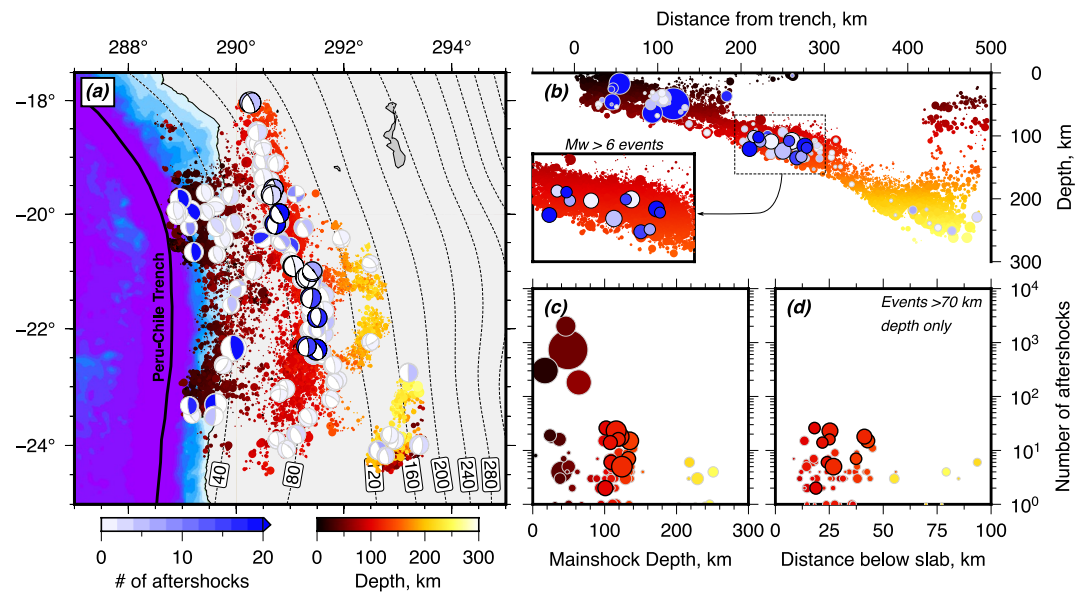


Figure 2. Aftershock productivity of moderate-magnitude earthquakes in northern Chile using the IPOC catalog of Sippl et al. (2018). (a) Map of the spatial distribution of the seismicity overlain with the focal mechanisms of the mainshocks taken from the gCMT catalog. The focal mechanisms are colored by the number of counted aftershocks. Mainshocks that are M_w 6.0–6.5 and at depths ≥ 70 km are highlighted by a black outline. Slab contours are from Slab 2.0 (Hayes et al., 2018). (b) Cross-section through the IPOC seismicity overlain by the mainshocks shown as blue circles. Mainshocks are scaled by magnitude. (c) Aftershock productivity as a function of mainshock depth for mainshocks across all depths. (d) Aftershock productivity as a function of depth below the slab surface for mainshocks with hypocentral depths > 70 km only.

shallow and intermediate-depth mainshocks using this data set. Therefore, we focus our analysis on the relative aftershock productivity amongst the population of intermediate-depth earthquakes that have similar magnitudes.

The majority of the large intermediate-depth earthquakes beneath northern Chile occur in a cluster in the depth range of 80–140 km and 200–300 km from the trench (Figure 2b). Within this cluster, the 12 largest $M_w > 6$ earthquakes have near-identical magnitudes, focal mechanisms, hypocentral depths, and are in similar parts of the slab, but can still have significant differences in the number of aftershocks they produce (Figure 2b, see inset). There is no clear change in the number of aftershocks with depth for events within the intermediate-depth cluster Figure 2c. Cabrera et al. (2021) suggested that the aftershock productivity may decrease systematically as a function of distance below the slab surface using six well-located mainshocks, though we did not find this pattern when considering our data set of 114 mainshocks (Figure 2d). The spatial heterogeneity in aftershock productivity even in this small study area suggest that the controls on aftershock productivity may vary on length-scales that are small compared to the location differences between mainshocks, which is equivalent to a few tens of kilometers.

Similar analyses of high-resolution regional earthquake catalogs have been performed for intermediate-depth earthquakes in Cascadia (Gomberg & Bodin, 2021) and Japan (Chu & Beroza, 2022). The analysis from Cascadia included 63 mainshocks and used a catalog complete down to $M_L = 1.9$. Gomberg and Bodin (2021) found that the aftershock productivity increased with mainshock magnitude and decreased with mainshock depth. A notable difference between Cascadia and northern Chile is that the background seismicity rate correlates weakly with the aftershock productivity in Cascadia, whilst we did not find this trend in either our global analysis or for northern Chile (Text S3 in Supporting Information S1). The analysis of aftershock productivity in Japan included 64 mainshocks and used the JMA catalog, which is complete to $M_{JMA} = 2.0$. Chu and Beroza (2022) found that the aftershock productivity of intermediate-depth earthquakes was consistently lower than shallow earthquakes of equivalent magnitude, and that aftershock productivity increased with magnitude. However, there was not enough variability amongst the intermediate-depth events to determine whether aftershock productivity varied with depth. Chu and Beroza (2022) found that around half of all events have no recorded aftershocks, whilst for those that do have aftershock sequences the aftershock productivity scales with the V_p/V_s ratio in the region. In northern Chile, we find more of a continuum of aftershock productivity, but our results support the view of Chu

and Beroza (2022) that some mechanism in addition to just the depth and magnitude of the mainshock is influencing the variability in aftershock productivity.

2.3. Summary of Aftershock Productivity Results

We find that the low aftershock productivity of intermediate-depth earthquakes compared to shallow earthquakes of equivalent magnitude is a robust result between both global and regional earthquake catalogs. For intermediate-depth earthquakes, the aftershock productivity increases systematically with mainshock magnitude as $\approx 10^{M_w}$, and we have shown tentative evidence that it decreases slightly as a function of depth. We interpret the increase in aftershock productivity with magnitude to reflect the fact that larger mainshocks having larger rupture areas A with $A \propto 10^{M_w}$ causing stress changes on a larger fault area, or in a larger volume, surrounding the mainshock rupture (Wetzler et al., 2016). Assuming that the number of faults within the slab remains constant with depth, the slight decrease in aftershock productivity with depth for earthquakes between 60 and 300 km implies that the mechanism that controls aftershock productivity is also itself depth dependent. However, an important conclusion is that there is still variability in the aftershock productivity of intermediate-depth earthquakes that cannot be explained by the magnitude of the mainshock and mainshock depth alone.

We did not find any robust evidence for systematic variations in aftershock productivity between different slab settings. For example, the aftershock productivity does not vary systematically with the background rate of seismicity within the slab. Rather, aftershock productivity seems to be heterogeneous at the scale of individual subduction zones and within individual slabs. The variability in aftershock productivity within the cluster of near-identical intermediate-depth earthquakes beneath northern Chile is the type example of this behavior, and which leads us to suggest that the mechanism that controls aftershock productivity may also be heterogeneous over length-scales of only a few tens of kilometres.

The low aftershock productivity of intermediate-depth earthquakes compared to shallow earthquakes of equivalent magnitude suggests fault systems within the slab are less sensitive to stress transfer than those within the shallow parts of the lithosphere. In the next section, we explore whether intraslab faults are also insensitive to slip on the subduction interface in major megathrust earthquakes.

3. Response of Intermediate-Depth Seismicity to Megathrust Slip

Intraslab faults will experience stress changes in response to slip on the megathrust (Lin & Stein, 2004). These stress changes have been suggested to modulate the frequency of earthquakes that accommodate down-dip extension or compression within the slab (Astiz et al., 1988; Dmowska et al., 1988; Lay et al., 1989). In particular, Astiz et al. (1988) argued that down-dip compressional earthquakes at intermediate depths are more frequent after megathrust earthquakes, and down-dip extensional earthquakes less frequent, as megathrust slip may cause incremental down-dip compression of the slab.

3.1. Stress Changes in Slabs Caused by Megathrust Slip

The stress changes caused by slip on a megathrust will vary throughout the slab, and may therefore modulate where earthquakes are triggered. Therefore, to test the conceptual model of Astiz et al. (1988) and inform our data processing strategy, we first performed a set of calculations to examine the stress changes caused by slip on the megathrust in different slab settings. We calculated the stress changes in two dimensions using the elastic dislocation model of Okada (1992) and a synthetic slip distribution on the slab surface defined by Slab 2.0 (Hayes et al., 2018). The two-dimensional approximation is reasonable given that, for $M_w > 8$ megathrust earthquakes, the rupture area is typically longer along-strike than it is wide down-dip (Allen & Hayes, 2017). In our models, slip on the slab surface extended from the up-dip edge of Slab 2.0–50 km depth, and had a trapezoidal distribution with slip tapering over a down-dip distance of 50 km toward the edge of the slip patch. Synthetic tests showed that applying more complex slip distributions derived from finite-fault slip inversions had little effect on either the amplitude or the geometry of the stress changes at distances >20 km from the megathrust, as long as the average amount and depth-extent of slip on the megathrust is accurate (Text S4 in Supporting Information S1). The results of these calculations for three different slab geometries (Japan, Kermadec and northern Chile) are shown in Figure 3.

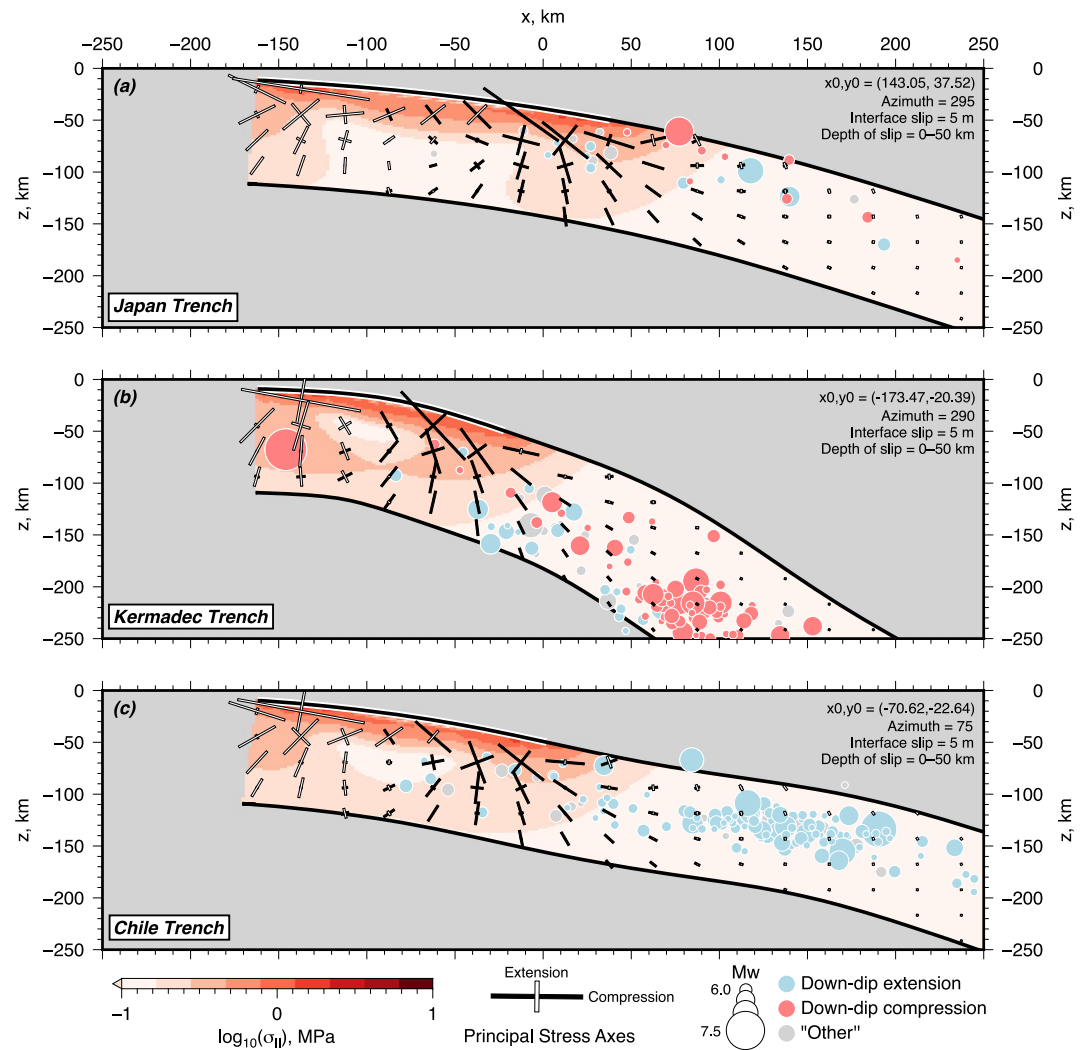


Figure 3. Stress changes imposed on the slab due to slip on the megathrust in regions with different slab geometries, including (a) Japan, (b) Kermadec, and (c) northern Chile. The slip distribution in each calculation is limited to between the section of the slab surface highlighted in white, has a peak of 5 m, and linearly tapers toward the up-dip and down-dip edge of the slip patch over a distance of 50 km. σ_{II} is the second invariant of the stress tensor, which represents the maximum shear stress imposed on faults within the slab. The principal stress axes show the geometry of the stress changes. Seismicity within 200 km of the slab profile is shown as circles scaled in size by the earthquake magnitude. The seismicity is taken from the global CMT catalog (Ekström et al., 2012), and is defined as down-dip extensional, down-dip compressional or “other” based on the criteria outlined in Section 3.2.

To first-order, slip on the megathrust adds a predominantly horizontal tensile stress within the outer-rise region, and adds a predominantly down-dip compressional stress in the area of slab down-dip of megathrust slip. The orientation of the principal stress axes rotate from being sub-parallel to the megathrust within the shallow parts of the slab to being oblique to the slab near its base. However, irrespective of the geometry of the slab, slip on the megathrust will lead to down-dip compression in the epicentral region of intermediate-depth earthquake generation (Figure 3).

The amplitude of the stress changes increases linearly with the average slip on the megathrust. Larger magnitude earthquakes will cause stress increases of a particular amplitude within a larger volume of the slab, and therefore potentially lead to a stronger signal of triggered seismicity. More generally, the largest stress changes occur at the tips of the slip area, which corresponds to the trench and, at its down-dip end, the brittle-ductile transition on the megathrust. Stress changes decrease with distance as approximately r^{-3} with distance from the megathrust (Okada, 1992), and the amplitude of the stress changes within the slab interior at intermediate depths are similar

to those within the outer-rise, where there is often extensive triggered seismicity after megathrust earthquakes (Bilek & Lay, 2018; Christensen & Ruff, 1983).

Overall, these physical models of stress change due to megathrust slip support the conceptual model of Astiz et al. (1988). In the next section, we therefore extend the original analyses of changes in intermediate-depth seismicity around the timing of major megathrust earthquakes from Astiz et al. (1988) and Lay et al. (1989) using the more temporally complete gCMT catalog (Dziewonski et al., 1981; Ekström et al., 2012).

3.2. Global Analysis

We focus our analysis on the largest megathrust earthquakes of $M_w \geq 8.0$ between 1990 and 2017, which provides us with a set of events that are likely to be on kinematically coupled sections of the megathrust and that were late in their earthquake cycle. Based on our modeling in Section 3.1, these large earthquakes are also the ones most likely to have led to changes in seismicity rates within the slab. For each large megathrust earthquake, we extracted all of the earthquakes surrounding the mainshock from the gCMT catalog with centroid depths in the range 60–300 km and that are within ± 200 km of the projection of the megathrust earthquake's T -axis in the down-dip direction of the slab. We then removed all earthquakes with centroids that are above the slab surface defined by Slab 2.0 (Hayes et al., 2018). We also repeated the analysis but without excluding events based on their position relative to the slab, given that both the slab surface and the earthquake centroid depths can be uncertain by ± 10 km or more, but found this had only a minor effect on the resulting patterns.

To assign each earthquake to either down-dip compression or extension, we filtered the events based on the angle between their P , T , and N -axes and the normal and dip vector of the slab derived from Slab 2.0. Earthquakes are associated with down-dip compression if the T -axis is within 45° of the slab normal, the N -axis makes an angle greater than 45° with the slab normal, and the P -axis makes an angle greater than 45° with the slab dip vector. The same filter was used to isolate down-dip extensional earthquakes, but with the constraint that the P -axis is within 45° of the slab normal vector. Earthquakes that do not fit these two conditions (denoted “other” in the analysis below) mostly accommodate along-strike deformation of the slab or shearing of the slab in the plane parallel to the slab dip direction (slab tearing). We also assess the temporal variability in these events to ensure that the method of data selection does not bias the results.

To examine changes in the frequency of intermediate-depth earthquakes associated with megathrust slip, we calculated the difference in the number of earthquakes before (N_b) and after (N_a) the mainshock at time t_0 . We then divide this by the total number of earthquakes in the period $[t_0 - \Delta t, t_0 + \Delta t]$, yielding a value $\Delta N/N = (N_a - N_b)/(N_a + N_b)$ that is in the range $[-1, 1]$. A value of 1 means all earthquakes of a particular mechanism occurred after the mainshock, whilst -1 means they all occurred before the mainshock. We calculated $\Delta N/N$ for all earthquakes with magnitude $M \geq M_c$ where M_c is in the range $[5.0, 6.0]$ and for Δt of 5 years or 10 years. This simple approach captures the rate changes without relying on any assumptions about the statistical distribution of seismicity in time, as a more complex approach is not warranted by the limited number of earthquakes.

The analyses of three different earthquakes illustrate the key results (Figure 4). For the 2011 M_w 9.1 Tohoku-oki earthquake, the largest event in the gCMT catalog, there are only 12 down-dip extensional and 21 down-dip compressional earthquakes at intermediate depths within 20 years of the mainshock (Figure 4a). All of the down-dip extensional earthquakes with $M_w \geq 5.5$ occurred prior to the mainshock, and there were no down-dip extensional earthquakes in the 10 years following the mainshock. Evidence for changes in the frequency of down-dip compressional earthquakes is less clear, as there are too few events (Figure 4a). Therefore, the extensional seismicity down-dip of the Tohoku-oki mainshock appears to follow the trend predicted by the model of Astiz et al. (1988). The slab down-dip of the 2001 M_w 8.1 Arequipa earthquake is far more seismogenic compared to Japan, with predominantly down-dip extensional seismicity as the slab bends into the mantle beneath the Andes (Figure 4b). The number of down-dip extensional earthquakes systematically increased following slip on the megathrust in the Arequipa earthquake, which is opposite to the trend expected if megathrust slip puts the slab into incremental down-dip compression and inhibits down-dip extensional earthquakes. The intermediate-depth seismicity down-dip of the 2006 M_w 8.2 Kermadec earthquake shows a different result again. In this region, the majority of the intermediate-depth earthquakes are associated with down-dip compression. We find no robust change in the frequency of down-dip extensional earthquakes caused by megathrust slip. However, the data suggests that the number of down-dip compressional earthquakes with $M_w \geq 5.5$ decreased after megathrust slip, which is again contrary to the prediction that megathrust earthquakes promote down-dip compressional seismicity.

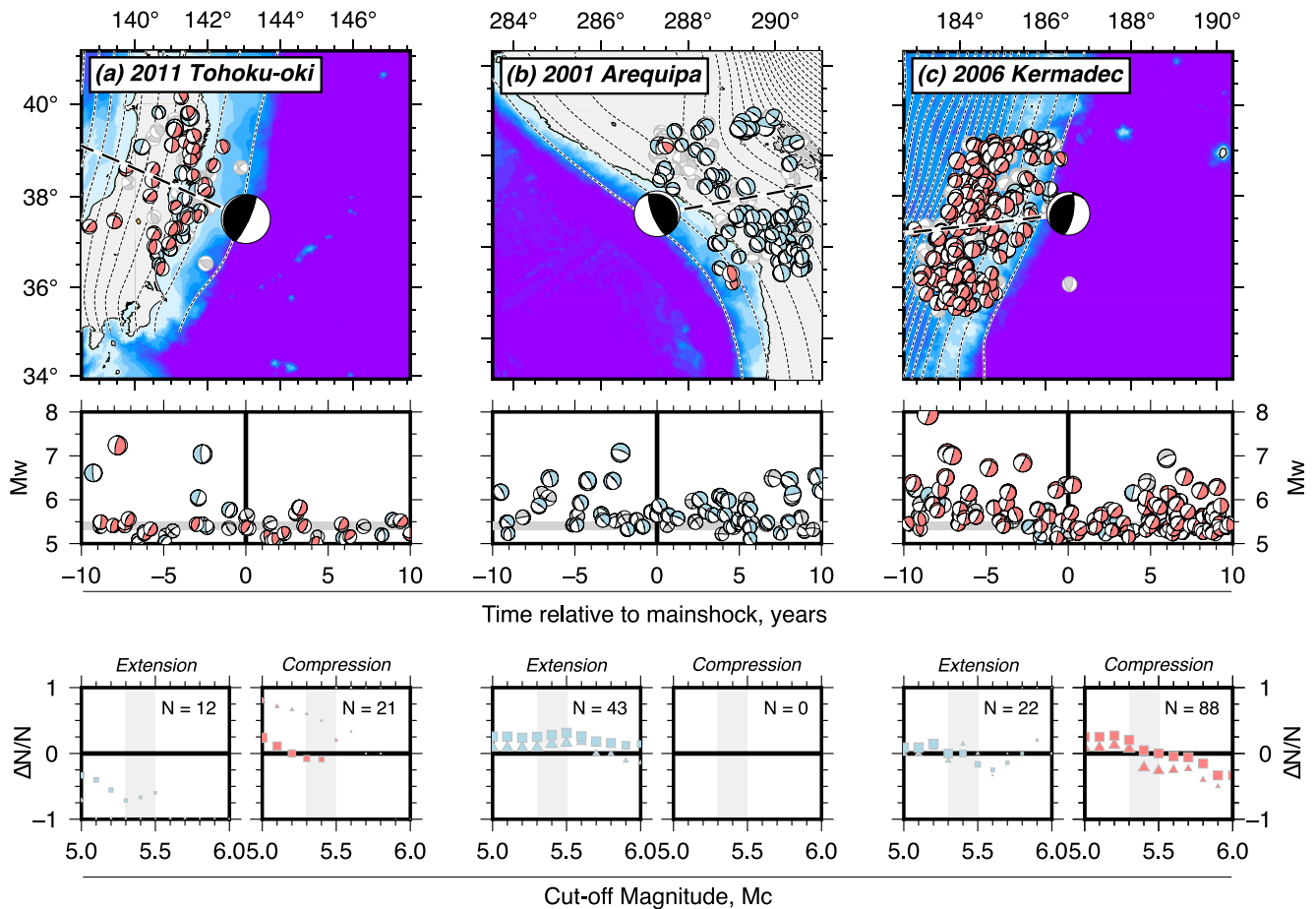


Figure 4. Examples of changes in intermediate-depth earthquake mechanisms before and after three major megathrust earthquakes. Mechanisms are colored red if they are related to down-dip compression, blue for down-dip extension and gray for along-strike deformation. Contours represent the depth to the slab surface from Slab 2.0 (Hayes et al., 2018) and are every 20 km. The middle panel is a time-series of earthquake mechanisms as a function of magnitude. The dark gray horizontal line represents the global magnitude of completeness of the gCMT catalog. The bottom panel shows the difference in the number of earthquakes after and before the megathrust event divided by the total number of earthquakes $\Delta N/N = (N_a - N_b)/(N_a + N_b)$, for down-dip extensional and compressional events. The vertical gray line shows the range of completeness for the gCMT catalog. Squares and triangles represent $\Delta N/N$ for the period 5 and 10 years either side of the mainshock, respectively. The size of the symbol is scaled by the number of earthquakes in that bin and decreases in size as the number of events in the bin gets smaller.

The three examples in Figure 4 demonstrate that changes in the frequency of earthquakes associated with down-dip extension or compression can occur around megathrust earthquakes, but they are not necessarily consistent between events. To further demonstrate this point, we performed the following test. For every mainshock j , we assign a decrease in rate $\Delta N/N < 0$ a value of $n_j = -1$ and an increase in rate $\Delta N/N > 0$ a value of $n_j = 1$ for a given time-span Δt relative to the mainshock and magnitude cut-off M_c . We then compute $\sum_{j=1}^k n_j(M_c, \Delta t)$ for all megathrust mainshocks $j = \{1, 2, \dots, k\}$. If there is a consistent pattern of rate increases after the mainshock, then $\sum_{j=1}^k n_j(M_c, \Delta t) > 0$, whilst a rate decrease would be associated with $\sum_{j=1}^k n_j(M_c, \Delta t) < 0$. This process is equivalent to a 1-dimensional simple random walk. In the case of the null hypothesis that an increase in seismicity is equally likely as a decrease, the expected value of $\sum_{j=1}^k n_j(M_c, \Delta t)$ is 0 and the standard deviation is \sqrt{k} . The results of this stacking process are shown in Figure 5.

For down-dip extensional seismicity the sum $\sum_{j=1}^k n_j(M_c, \Delta t)$ is similar to the expected value for the null hypothesis (Figure 5a), suggesting there is no consistent change in down-dip extension of the slab after megathrust earthquakes. Down-dip compressional seismicity does typically increase after megathrust earthquakes, but only for intermediate-depth earthquakes with $M_w \leq 5.5$ (Figure 5b), which is around the magnitude of completeness of the gCMT catalog (Kagan, 2003). The smallest M_w 5 earthquakes are also likely to have the largest depth and mechanism uncertainties (Wimpenny & Watson, 2020), and so thrust-faulting on the megathrust may also be incorrectly assigned to being within the slab. The amplitude of the deviation from the expected value for the null

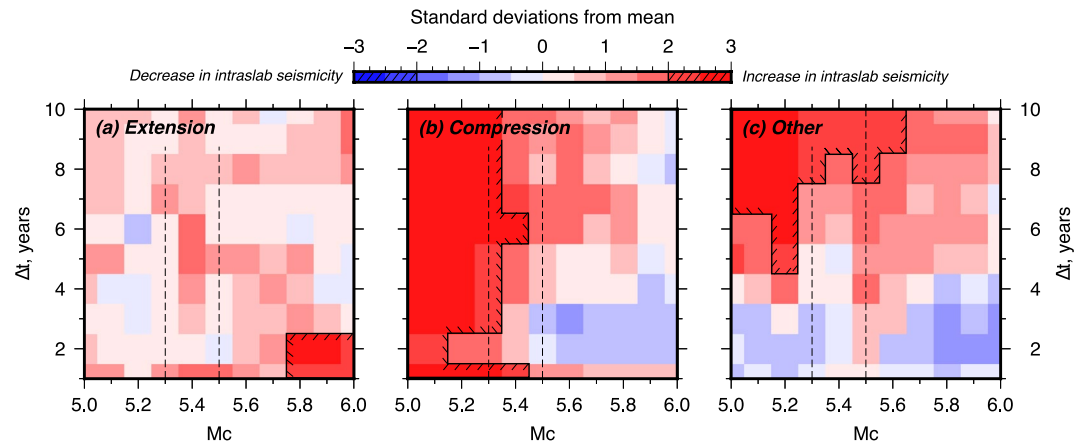


Figure 5. Compilation of changes in the frequency of intermediate-depth earthquakes following megathrust slip as a function of magnitude cut-off M_c and time-span Δt for (a) down-dip extensional, (b) down-dip compressional, and (c) other types of earthquakes. The color in each panel represents the number of standard deviations from the mean distance that the summation reaches in k steps, equivalent to $\sum_{j=1}^k n_j / \sqrt{k}$. Given the null hypothesis is that an increase and a decrease in earthquake frequency are both equally likely, the expected value of $\sum_{j=1}^k n_j / \sqrt{k}$ is zero. The vertical dashed lines represent the approximate range in magnitude of completeness of the gCMT catalog. The solid black line marks the 2 standard deviations boundary, with ticks on the inside of the boundary enclosing regions where the changes in earthquake frequency are unlikely to arise due to chance.

hypothesis for earthquakes $M_w > 5.5$ is smaller than 2 standard deviations, therefore we cannot reject the hypothesis that these changes in earthquake frequency are random when only considering events above the magnitude of completeness. Given that down-dip extension, compression, and other types of earthquake mechanisms at intermediate-depths generally increase in frequency in the 5–10 years after a mainshock (Figures 5a–5c), and the increase becomes more robust for longer time-spans Δt , then these trends most likely reflect the increase in the gCMT catalog completeness through time.

In summary, we find no robust evidence in the gCMT catalog for systematic changes in the frequency of moderate-to-large magnitude earthquakes that accommodate down-dip deformation of the slab in the intermediate-depth range. In the next two sections, we test whether the apparent lack of triggered intraslab seismicity might reflect the limited number of earthquakes within the gCMT catalog by focusing on two regions with extensive intraslab seismicity and high-quality regional catalogs.

3.3. Regional Analysis: Japan

Japan has the highest-resolution earthquake catalog of any subduction zone due to the dense onshore seismic network, and is therefore an ideal natural laboratory for this type of analysis. Delbridge et al. (2017) previously reported an increase in intermediate-depth seismicity down-dip of the rupture area of the 2011 Tohoku-oki earthquake in the upper plane of the double-seismic zone (DSZ) recorded by the regional earthquake catalog, which consists mostly of compressional earthquakes accommodating unbending of the Pacific plate. Our analysis of the earthquake moment tensors from the gCMT catalog failed to identify such a trend (Figure 4a). We therefore re-analyzed the frequency variations of intermediate-depth earthquakes recorded in the JMA catalog down-dip of the Tohoku-oki rupture area (Figures 6a and 6b). A total of 6,595 intermediate-depth earthquakes occurred in this region between 2006 and 2019 that are >100 km from the trench and >60 km deep, and which are larger than the magnitude of completeness of the catalog ($M_{JMA} = 2.0$). We assigned events to the upper or lower plane of the DSZ by binning the event depths relative to Slab 2.0 as a function of distance from the trench and fitting a Gaussian mixture model to the relative depth distributions.

To examine changes in the earthquake frequency, we calculated the average earthquake rate in the upper and lower plane of the DSZ using a moving window that has width T and moves in steps Δt . The results shown in Figures 6b–6d use $T = 0.2$ years and $\Delta t = 0.05$ years. From this moving window analysis, we confirm there is a spike in the frequency of earthquakes assigned to the upper plane within a month of the Tohoku-oki mainshock, with the rate increasing from ~ 0.5 earthquakes per day to nearly 6 per day (Figure 6c). There is no clear change in the frequency of

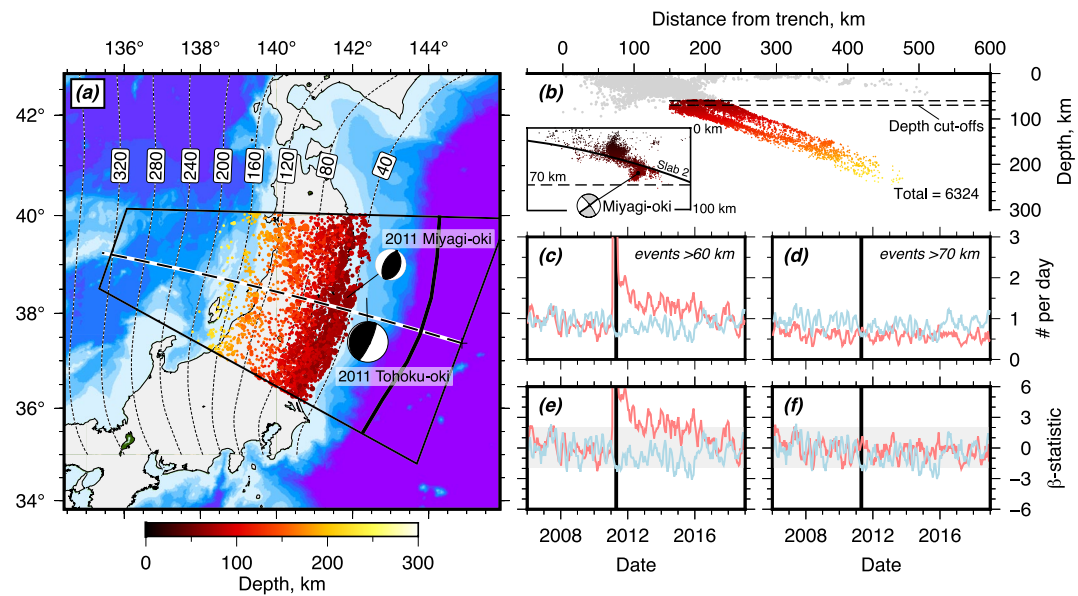


Figure 6. Temporal variations in intermediate-depth seismicity in response to the 2011 M_w 9.1 Tohoku-oki earthquake. (a) Spatial distribution of seismicity used in the analysis from the JMA catalog. Contours of the slab surface are shown as black-dashed lines from Slab 2.0 (Hayes et al., 2018). (b) Cross-section through the seismicity with the two depth cut-offs used in the analysis at 60 and 70 km shown as black dashed lines. Inset is a zoom-in of the seismicity within ± 1 month of the 7 April 2011 Miyagi-oki earthquake. The aftershocks of the Miyagi-oki earthquake clearly extend 10–15 km below the slab surface, but remain shallower than 70 km depth. (c) Average number of earthquakes per day in the upper plane (light red) and lower plane (light blue) of the double-seismic zone (DSZ) for all events >60 km depth. The time-series is calculated using a sliding window of length 0.2 years and time step 0.05 years. The vertical black line marks the timing of the Tohoku-oki mainshock. (d) Equivalent plot to (c), but for all events >70 km. (e) and (f) show the β -statistic of Matthews and Reasenber (1988) for all events >60 km and >70 km depth, respectively. If β exceeds 2, this is equivalent to the earthquake rate deviating more than 2 standard deviations from background, with the background defined by the seismicity rate during the period 2006–2011.

lower-plane earthquakes over the same period. The peak seismicity rate in the upper plane occurred 1 month after the mainshock and decayed over 7 years before returning to the background rate in 2018. However, this result is extremely sensitive to the cut-off depth (Figure 6d). For an identical analysis of earthquakes that have depths >70 km, the spike in earthquake frequency disappears and there is no clear deviation from the pre-Tohoku seismicity (Figure 6e).

The large number of earthquakes in the JMA catalog, and the relatively stable rate of seismicity prior to Tohoku, allows us to test the statistical significance of the seismicity rate changes using the β -statistic of Matthews and Reasenber (1988). The β -statistic is calculated as $\beta = (N - N_0)/\sigma_0$ where N is the observed number of earthquakes within a sliding window of length T , and N_0 and σ_0 are the mean and standard deviation of the number of earthquakes within time windows of length T selected randomly from within the reference time period (in our case 2006–2011). The results of the β -statistic analysis applied to the JMA data shows that there are no variations in the earthquake frequency for events >70 km that are greater than 2 standard deviations from the pre-Tohoku seismicity (Figure 6f). An analysis of the seismicity in the ISC reviewed catalog from the same region, which support our observations made using the JMA catalog, is discussed in Text S5 in Supporting Information S1.

Further investigation revealed that the seismicity contributing to the spike in earthquake frequency in the upper plane in Figure 6c mostly derived from the region of the 7 April 2011 M_w 7.2 Miyagi-oki reverse-faulting earthquake, which ruptured the slab at ~ 55 – 65 km depth less than a month after the Tohoku-oki mainshock. Removing the seismicity within 50 km of the Miyagi-oki earthquake suppresses the spike in the intermediate-depth seismicity rate (Text S5 in Supporting Information S1). It is also possible that the ~ 5 – 10 km uncertainties in earthquake hypocentral depths for small earthquakes in the JMA catalog mean that some aftershocks occurring at the down-dip edge of the megathrust, or within the overriding plate, are mislocated and have been incorrectly assigned to the upper plane of the DSZ (e.g., Sippl et al., 2019). To test this possibility, we removed all events that are within 10 km of the plate interface from the analysis, which also suppresses the spike in seismicity rate related to the Tohoku-oki and Miyagi-oki earthquakes (Text S5 in Supporting Information S1). Therefore, we

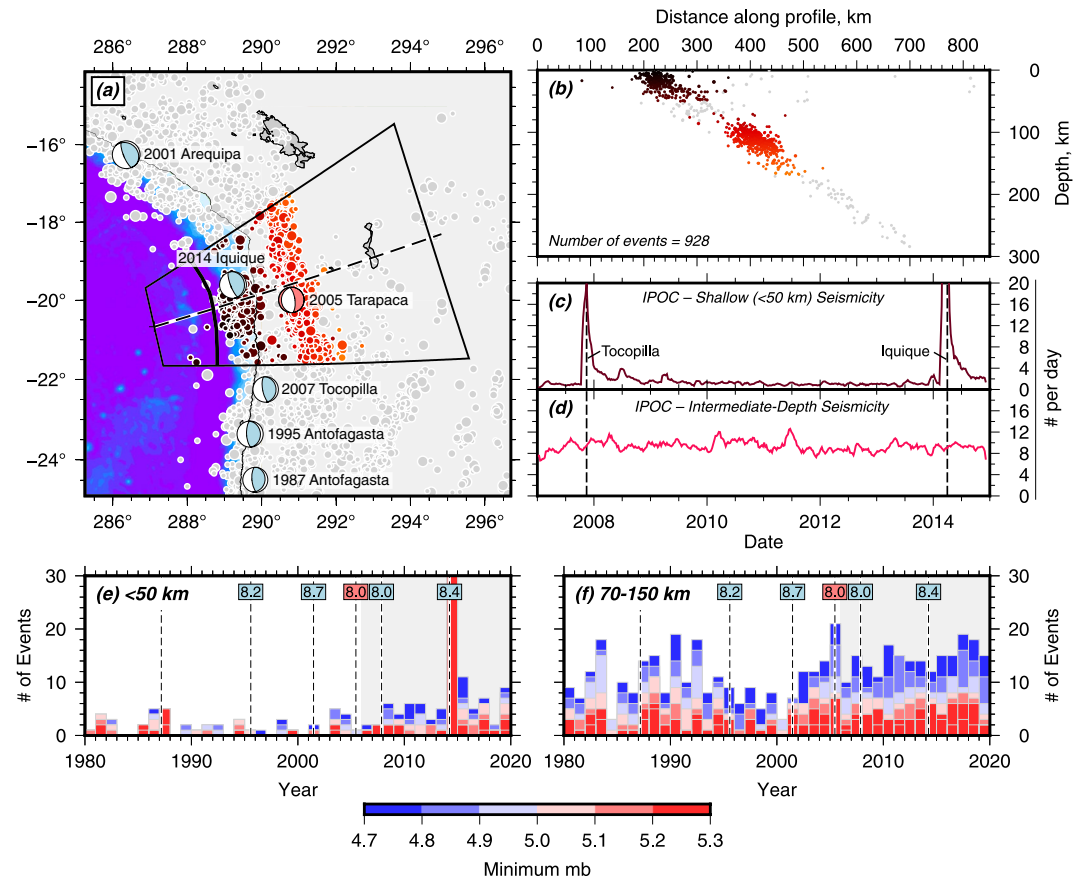


Figure 7. Overview of seismicity in northern Chile between 1980 and 2020. (a) Map view of the distribution of seismicity from the ISC catalog with $m_b \geq 4.7$ with the focal mechanisms of the largest mainshocks. Gray circles represent earthquake hypocenters, and colored circles represent earthquakes used in the analyses in (b, e, f). Dark colored circles are shallow earthquakes and red-orange colored circles are intermediate-depth earthquakes. (b) Cross-sectional view of the seismicity projected onto the black-dashed path in (a) showing the cluster of seismicity at ~ 400 km distance along the profile. (c) Temporal evolution of shallow (< 50 km) seismicity in northern Chile from the IPOC catalog of Sippl et al. (2018) calculated using a sliding window of width 0.1 year and time steps of 0.02 years (d) Same as (c), but for the intermediate-depth seismicity between 70 and 300 km depth. (e) and (f) show histograms of the number of earthquakes in the ISC catalog with $m_b > M$ each year for the shallow and intermediate-depth seismicity, respectively. The area in gray marks the installment of the IPOC network in northern Chile in 2006. Vertical dashed lines mark the timing of major earthquakes in the region and their magnitudes, with megathrust events represented by a light blue box and intraslab events by a light red box.

conclude that the change in earthquake frequency identified by Delbridge et al. (2017) may not indicate a slab-wide increase in intermediate-depth earthquake frequency in response to the 2011 Tohoku-oki earthquake, but rather the aftershock sequence of the Miyagi-oki earthquake (Figure 6b, inset). This difference is important, because it suggests that the majority of faults that are definitively within the slab are insensitive to the stress changes caused by megathrust slip in the Tohoku-oki earthquake.

3.4. Regional Analysis: Northern Chile

Megathrust slip has also been proposed to modulate intermediate-depth seismicity in northern Chile. Jara et al. (2017) suggested that the 1995 Antofagasta and 2014 Iquique megathrust earthquakes were followed by periods of reduced moderate-magnitude seismicity at intermediate depths beneath northern Chile, whilst the 2005 Tarapaca intraslab earthquake was followed by 9 years of increased seismicity at both shallow and intermediate depths (Figures 7a and 7b). Since Jara et al. (2017)'s original analysis, Sippl et al. (2018) has published an earthquake catalog spanning 2006–2015 in northern Chile that is complete down to $M_L = 2.8$, which allows us to examine the changes in intermediate-depth earthquake frequency before and after the Iquique earthquake in more detail. We calculated the earthquake rate through time using the moving window analysis described in

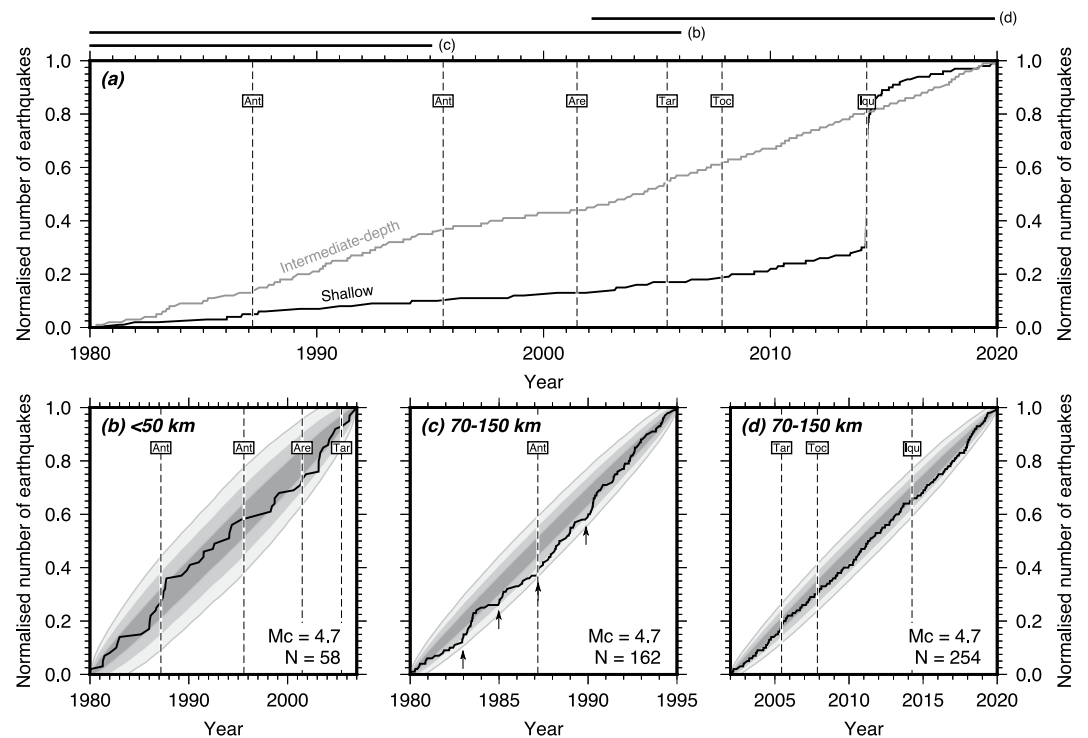


Figure 8. Cumulative distribution of shallow and intermediate-depth earthquakes in northern Chile shown in Figure 7a. (a) Cumulative distribution between 1980 and 2020 of events $m_b \geq 4.7$. Major ($M_w \geq 7.5$) megathrust and intermediate-depth earthquakes are shown by vertical dashed lines, with Ant = Antofagasta, Are = Arequipa, Tar = Tarapaca, Toc = Tocopilla and Iqu = Iquique (b–d) Cumulative distributions of seismicity over particular periods of time compared to the predictions of time-randomised catalogs. The gray polygons show the area in which 67%, 95% and 99% of catalogs with the same number of events N but randomised earthquake times would plot. The confidence intervals are wider for catalogs with fewer events. In (c) vertical arrows point out distinct changes in the frequency of earthquakes that do not correlate with any major earthquakes. The equivalent plot for the declustered catalog is shown in Figure S14 in Supporting Information S1.

Section 3.3, but found no significant deviations in the frequency of intermediate-depth seismicity following the 2014 Iquique earthquake or the 2007 Tocopilla earthquake (Figures 7c and 7d).

The catalog of Sippl et al. (2018) is too short to capture any of the multi-year trends in earthquake frequency identified by Jara et al. (2017). Therefore, we re-analyzed the temporal variations in seismicity in northern Chile between 1980 and 2020 using four more years of data in the ISC's reviewed catalog than were available to Jara et al. (2017) (Figure 7a). An important limitation in comparing temporal variations in the shallow and intermediate-depth seismicity in this region is that the ISC catalog's magnitude of completeness is higher for shallow earthquakes that are offshore ($m_b = 4.7$) than for intermediate-depth earthquakes that are beneath the land ($m_b = 4.3$; see Text S6 in Supporting Information S1). To ensure that this spatial variability in completeness does not bias our analysis, we only studied events with $m_b \geq 4.7$, which for the region shown on Figure 7 includes 925 earthquakes between 1980 and 2020.

The annual variations in the frequency of shallow (<50 km) and intermediate-depth (70–170 km) earthquakes are shown as histograms in Figures 7e and 7f, and as a cumulative distribution in Figure 8a. We plot the data as histograms, as opposed to using the moving window analysis of Section 3.3, because there are so few earthquakes above the magnitude of completeness. The depth intervals were selected to closely replicate the analysis of Jara et al. (2017). Unlike Jara et al. (2017), however, we describe the trends in the undeclustered catalog, and present the equivalent analyses of the declustered catalog in Text S6 in Supporting Information S1. We take this approach, because the deficiency of intermediate-depth aftershock sequences means that declustering has little effect on the trends in intermediate-depth earthquake frequency through time.

There is little shallow seismicity in northern Chile between 1980 and 2007 with typically fewer than 5 earthquakes per year with $m_b \geq 4.7$ (Figure 7e), which makes identifying any changes in earthquake frequency during this period difficult. There are so few events in 1980–2007 that the cumulative earthquake distribution with time

is not significantly different (<2 standard deviations) from synthetic catalogs that contain the same number of events but with randomised times (Figure 8b), suggesting the shallow seismicity contains no robust information about temporal changes in earthquake frequency in response to the 1995 Antofagasta, 2001 Arequipa, or 2005 Tarapaca earthquakes. Between the 2007 Tocopilla and 2014 Iquique earthquakes the annual number of shallow earthquakes increased (Figure 7e), which is associated with the well-documented foreshock sequence of the Iquique earthquake (Ruiz et al., 2014). The Iquique earthquake is then followed by an extensive aftershock sequence that lasts until the end of the catalog in 2020 (Figures 7e and 8a).

At intermediate depths the seismicity is more frequent and variable through time (Figure 7f). Between 1980 and 1995 the annual earthquake frequency changes from year-to-year (Figure 7f), but does not deviate from the behavior of time-randomised catalogs (Figure 8c). During 1980–1995, pulses of seismicity occurred in 1983, 1985, and 1990 that were not associated with a large megathrust or intermediate-depth earthquake (Figure 8c, black arrows). After 1995, there are two distinct changes in the earthquake frequency that last for multiple years: first a decrease around the timing of the 1995 Antofagasta earthquake and then an increase around the timing of the 2001 Arequipa earthquake (Figure 7f). This period of seismic quiescence at intermediate-depths between 1995 and 2001 appears to be robust in northern Chile for magnitudes at least 0.5 units larger than the catalog completeness (Figure 7f). After 2001, we found no evidence for robust changes in the intermediate-depth earthquake frequency caused by the 1987 Antofagasta, 2007 Tocopilla, and 2014 Iquique earthquakes (Figures 8c and 8d).

Our observations support the view that temporal changes in intermediate-depth earthquake frequency in northern Chile did occur, and in some cases lasted for multiple years. However, they are not consistently associated with megathrust earthquakes or large intermediate-depth earthquakes. If there were a consistent physical reason for the frequency changes in response to megathrust slip, then it is unclear why they should occur for only two megathrust events out of six between 1980 and 2020. In addition, using the longer earthquake catalog, we found that the 2014 Iquique megathrust earthquake had no resolvable effect on the frequency of intermediate-depth earthquakes within the slab directly down-dip from the rupture area. Therefore, we argue that large megathrust earthquakes are not the cause of changes in earthquake frequency at intermediate depths beneath northern Chile.

4. Discussion

4.1. Stress Sensitivity of Intermediate-Depth Seismicity

We initially set out to reconcile two contrasting views of intermediate-depth seismicity: one that suggested intraslab fault systems are sensitive to small stress changes associated with megathrust earthquakes, and another that suggested intraslab fault systems are insensitive to the stress changes caused by large intraslab earthquakes. Our analyses support the view that intermediate-depth seismicity within subducting slabs is relatively insensitive to static stress transfer as a result of slip in large earthquakes with typical stress drops (~ 1 –50 MPa; see Allmann & Shearer, 2009; Poli & Prieto, 2016; Tian et al., 2022). This insensitivity is manifest as consistently low aftershock productivity of intermediate-depth earthquakes, and no consistent triggering of down-dip compressional seismicity, or inhibition of down-dip extensional seismicity, within slabs following megathrust slip. We also did not find any clear evidence that the sensitivity of intraslab faults to static stress transfer varies systematically between subduction zones with different slab conditions.

The lack of seismicity triggered by static stress transfer at intermediate depths is similar to lack of seismicity triggered by earthquakes on oceanic transform faults (Boettcher & Jordan, 2004), but in stark contrast to the extensive seismicity that is triggered within the outer rise and outer trench-slope region following many major megathrust earthquakes that slip to the trench (Bilek & Lay, 2018; Christensen & Ruff, 1983). Earthquakes in the outer rises also have aftershock productivities similar to earthquakes of equivalent magnitude within the continents (Dascher-Cousineau et al., 2020). This comparison between intermediate-depth and outer-rise seismicity is informative, because the earthquake sources are in similar host material, just at different confining pressures and temperatures. Therefore, the difference in sensitivity to stress change between outer-rise and intermediate-depth seismicity does not appear to be related to the distinct composition of the oceanic lithosphere. Rather, it suggests that either: (a) the fault systems in the subducted oceanic lithosphere are not as close to failure as those at the outer rise, or (b) that the mechanism of earthquake generation at intermediate depth is not as sensitive to changes in static stress on the order of earthquake stress drops. This new view of the sensitivity of fault systems within subducted oceanic lithosphere places constraints on the mechanics of earthquake generation at intermediate

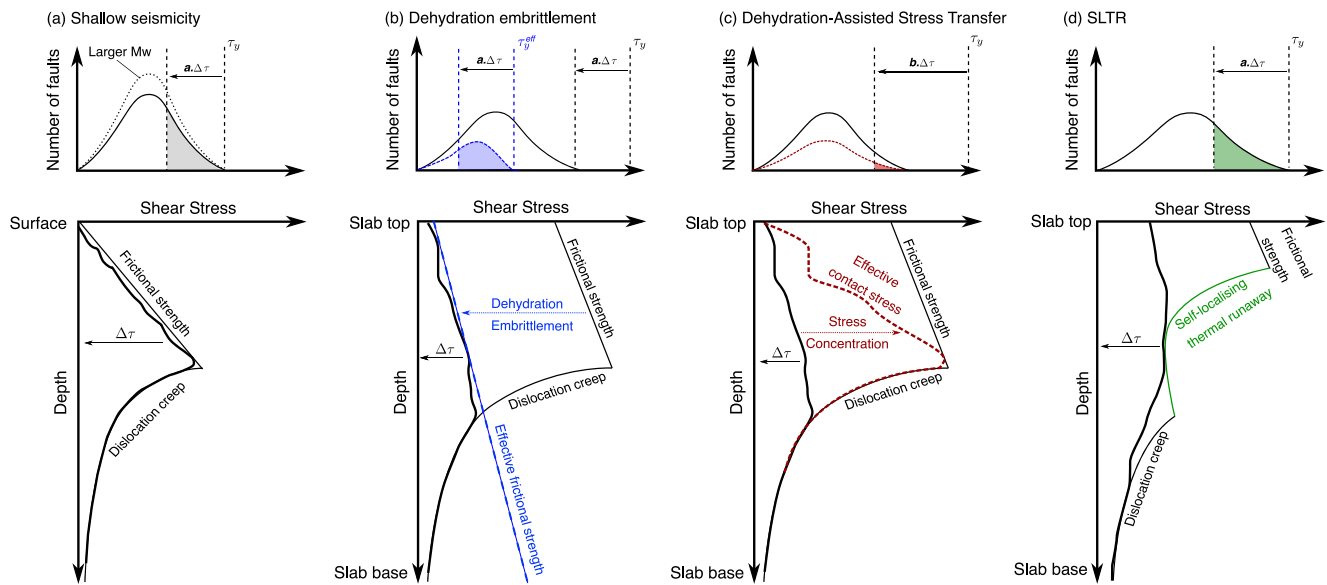


Figure 9. Sketch of the effect of stress transfer from an earthquake stress drop of amplitude $\Delta\tau$ on the triggering of nearby seismicity for (a) shallow earthquakes, and intermediate-depth earthquakes generated by (b) dehydration embrittlement, (c) dehydration-assisted stress transfer, and (d) self-localizing thermal runaway (SLTR). For each mechanism, the top row shows the shear stress distribution on a population of seismogenic faults within a fixed (arbitrary) volume around the mainshock, where τ_y is the maximum failure stress for a given failure mechanism. In (b) and (c) the maximum failure stress would be dry olivine friction, or the effective failure stress τ_y^{eff} for faults containing highly pressurized fluids. In (c) the maximum failure stress would be the stress needed to drive self-localizing thermal runaway. The colored region shows schematically the number of faults that would fail in aftershocks in response to a fixed stress transfer. The bottom row shows the failure strength envelope. The envelope shape in (d) is modified from John et al. (2009).

depths, and the interplay between the source of stress and the mechanism allowing the release of stress in earthquakes on intraslab faults, which we explore further below.

4.2. Fault Mechanics of Intermediate-Depth Seismicity

Based on the earthquake catalog data, and recent work on the source properties of intermediate-depth earthquakes, any model of intermediate-depth seismicity should account for three observations.

1. Intermediate-depth earthquake stress drops (for both mainshocks and aftershocks) should be of a similar order of magnitude to those at shallow depth (Allmann & Shearer, 2009; Poli & Prieto, 2016; Tian et al., 2022).
2. The response of intermediate-depth seismicity to stress changes caused by earthquake stress drops must be limited, in order to explain the observations of low aftershock productivity and the low sensitivity of intraslab seismicity to slip on the megathrust interface.
3. There must be *some* capacity to generate limited aftershocks after intermediate-depth earthquakes, and this capacity should broadly scale with mainshock depth and mainshock magnitude.

For shallow faulting, the clock-advance model has proven a simple way of interpreting the sensitivity of fault systems to static stress transfer (Hainzl et al., 2010; King et al., 1994). In this model aftershocks reflect earthquakes on faults that would have eventually ruptured in response to slow stress accumulation, but occurred earlier than expected due to an additional source of stress. A stress drop of $\Delta\tau$ due to slip in an earthquake leads to stress transfer onto the surrounding faults of magnitude $a_j \Delta\tau$, where a_j denotes a vector containing the elastic constants, distance, and relative geometry of the newly stressed fault (Hainzl et al., 2010). If the faults surrounding the mainshock have a stress distribution τ_j and a yield stress τ_y , then any fault patches around the mainshock where $\tau_j + a_j \Delta\tau > \tau_y$, will rupture in an aftershock (Figure 9a). In Figure 9a we assume that τ_j follows a distribution that is symmetrical about the mean stress, and has a mean value set by the requirement for equilibrium. We also assume that τ_y is roughly constant. Under these assumptions, fewer aftershocks would be produced if the static stress transfer from the mainshock $a_j \Delta\tau$ is a smaller fraction of the failure stress τ_y , or if the shape of the fault stress population becomes more skewed toward lower stresses. More aftershocks will be produced for larger magnitude

earthquakes, because the volume of material around the mainshock that experiences stress changes will be larger meaning the curve in Figure 9a will be taller.

A simple prediction of the clock-advance model is that for a given background seismicity rate r and stressing rate $\dot{\tau}$, then a change in static stress $\Delta\tau$ should lead to a change in the number of earthquakes in a region proportional to $r\Delta\tau/\dot{\tau}$. Our analysis suggests that aftershock productivity for intermediate-depth earthquakes does not correlate with the background seismicity rate within the slab (see also Chu & Beroza, 2022; Sippl et al., 2019). Similarly, the aftershock productivity does not correlate with the down-dip gradient in slab curvature, which is a proxy for the bending-related loading rate of faults within the slab (Sandiford et al., 2020). In addition, areas where intermediate-depth seismicity is particularly common (e.g., northern Chile) are not more sensitive to earthquake stress changes than places where the slab has relatively few earthquakes (e.g., central Japan). We suggest these departures from predictions of the clock-advance model may indicate that the stresses sustained by the intraslab fault population are significantly below the failure stress, and changes in the failure stress through fault weakening mechanisms far exceed the stress transfer from earthquake stress drops. The modifications to the clock-advance model for the three main weakening mechanisms proposed to enable intermediate-depth seismicity (dehydration embrittlement, dehydration-assisted stress transfer, self-localizing thermal runaway) are shown in Figures 9b–9d. We discuss each mechanism, and its ability to account for the three features of intermediate-depth seismicity, in turn below.

4.2.1. Dehydration Embrittlement

Dehydration embrittlement involves the weakening of fault zones through the build up of highly pressurized fluids released by the breakdown of hydrous mafic minerals during prograde metamorphism (Figure 9b). For this mechanism, the low stress drops in intermediate-depth earthquakes compared to the stresses required for frictional failure on a fault formed of dry olivine at equivalent depths (~ 1 GPa at 100 km depth) may either reflect partial stress release, the low shear stresses needed to break faults with a low effective strength, or some combination of both of these.

To simplify the representation of dehydration embrittlement in Figure 9b, we consider two populations of faults within the slab: those that contain highly pressurized fluids, and those that do not. Faults containing pressurized fluid are breaking in earthquakes at a low failure stress (Figure 9b), whilst dry faults will be far from their failure stress because the finite size of the forces acting on the slab can only load them to a fraction of their failure stress. For the dry fault population, static stress transfer is unlikely to trigger aftershocks, because most of the faults support stresses that are a small fraction of the failure stress (Figure 9b, black curve). In contrast, stress transfer could trigger slip on the fault population containing pressurized fluids, with the number of aftershocks being related to the number of faults that have been able to trap and build up high fluid pressures (Figure 9b, blue curve). Pervasive dehydration embrittlement, in which most faults in the slab contain near-lithostatic pore fluids, seems unlikely, as this would cause the intraslab faults to be sensitive to stress transfer, and we would expect an aftershock productivity similar to that seen in the shallow crust or higher.

Recent work has highlighted the link between aftershock productivity in the subducted Pacific slab beneath Japan and the V_p/V_s structure of the surrounding medium (Chu & Beroza, 2022), with higher aftershock productivity linked to higher V_p/V_s ratios and by inference more fluid, which supports this model. The effects of dehydration embrittlement are expected to be spatially heterogeneous due to its dependence on the availability of hydrous minerals and the trapping of the released fluid in faults, then this mechanism has the capacity to account for the spatial variability in aftershock productivity within slabs. Dehydration embrittlement can therefore account for the observations outlined in Section 4.2.

4.2.2. Dehydration-Assisted Stress Transfer

An alternative mechanism is dehydration-assisted stress transfer, where the loss of load-bearing capacity of hydrous minerals within a mixed-composition aggregate leads to the support of the total force acting on a fault onto a fraction of its surface area, allowing the fault to locally reach its failure stress (Ferrand et al., 2017) (Figure 9c). Whilst the failure stress and stress drops at contact level for this mechanism need to be extremely high (500–1,000 MPa), fault-averaged stress drops could be far lower if the fault can rupture through patches of weaker hydrous minerals at low shear stresses to account for the ~ 1 –50 MPa seismologically observed stress drops. Melting of the rupture plane at high stresses could also lead to a proportion of the stress release being accommodated aseismically as ductile shearing during the latter stages of slip, after an initial seismically radiating phase. The resulting stress transfer onto the surrounding faults would be moderated by elastic parameters, the

relative location and fault geometry, plus an additional factor describing the degree to which dehydration-assisted stress transfer concentrates stresses at the contact level ($b_j \Delta \tau$; Figure 9c).

As with dehydration embrittlement, the fault population will support average stresses that are significantly lower than the failure stress of faults containing dry olivine (Figure 9c, black curve). Following a mainshock the stress transfer onto the surrounding faults will be a small fraction of the total fault strength, but will be boosted by the focusing of the stress onto small asperities described by the factor b_j . The controls on aftershock productivity will therefore be similar to the dehydration embrittlement mechanism described above, as it will depend on the degree to which the surrounding material had already dehydrated, and therefore the proportion of the fault population within the slab that can generate the locally high contact stresses needed for failure (Figure 9c, red curve). Zero or low aftershock productivity will occur where the majority of the weak, hydrous phases have broken down into stronger anhydrous phases, meaning that the factor b_j is smaller. The relative insensitivity of intermediate-depth seismicity to slip on the subduction interface is a result of the stress transfer being a smaller fraction of the failure stress compared to shallow faulting (Figure 9c). Hence, dehydration stress-transfer can also match the three observational requirements described above.

4.2.3. Self-Localizing Thermal Runaway

The final weakening mechanism is self-localizing thermal runaway, in which creep in shear zones causes shear heating and the development of ductile instabilities that relax elastic strain (Hobbs & Ord, 1988; Ogawa, 1987). Numerical models of self-localizing thermal runaway suggest that the stress drops generated by an earthquake are a significant fraction of the fault's failure stress (often ~500–1,000 MPa at ~1 GPa confining pressure), as the positive feedback between strain and shear heating drives runaway failure that relaxes the majority of the elastic strain stored around the fault (John et al., 2009; Kelemen & Hirth, 2007). Not all of the stress drop and strain release may be seismogenic, and therefore this mechanism might be consistent with the low seismologically determined stress drops. However, the resulting stress transfer onto surrounding fault systems $a_j \Delta \tau$ should be a larger fraction of the failure stress than for the dehydration-based mechanisms described above (Figure 9d).

The self-localizing thermal runaway weakening mechanism is mostly dependent on the stress state of the given shear zone, and does not require any additional chemical processes to weaken the fault. We would not expect to see sensitivity of intermediate-depth seismicity to the shallow, lower-stress drop megathrust earthquakes because the fault failure stress is much larger than the static stress transfer. However, we might expect aftershock productivity to be similar at intermediate-depths to shallow depths, because the ratio between the amplitude of the static stress transfer $a_j \Delta \tau$ and the fault failure stress τ_y will be similar to that at shallow depths (Figure 9d). Therefore, self-localizing thermal runaway is less consistent with our observations of low intraslab aftershock productivity for intermediate-depth earthquakes.

5. Conclusions

Intermediate-depth earthquakes produce fewer aftershocks compared to shallow (<60 km) earthquakes of similar magnitude. The areas of intermediate-depth seismicity down-dip of major megathrust earthquakes are also insensitive to the static stress transfer on the order of earthquakes stress drops caused by megathrust slip. We interpret the relative insensitivity of intermediate-depth seismicity to static stress transfer to suggest that faults within the slab are further from their failure stress than is typical for shallow fault systems. It follows that the availability of the weakening mechanism is the likely control on intermediate-depth aftershock productivity, and this mechanism is heterogeneous over length-scales of a few tens of kilometres to account for the variability in aftershock productivity within slabs. We suggest dehydration-related weakening mechanisms are most consistent with these observations.

Data Availability Statement

All data used in this study are freely available. The ISC catalogue is available from <https://doi.org/10.31905/D808B830>, the gCMT catalogue is available from <https://www.globalcmt.org/>, the JMA catalogue is available from https://www.data.jma.go.jp/svd/eqev/data/bulletin/index_e.html, and the IPOC catalogue is available from <https://doi.org/10.5880/GFZ.4.1.2018.001> (all last accessed December 2022). All of the codes needed to reproduce the aftershock productivity results and analysis of seismicity rates through time are available from <https://doi.org/10.5281/zenodo.7817786>.

Acknowledgments

The authors were supported in this work by the Royal Society under URF/R1180088 and R/FERE/210041. SW and TJC were also supported through COMET, the UK Natural Environment Research Council's Centre for the Observation and Modelling of Earthquakes, Volcanoes, and Tectonics. We thank Jorge Jara for useful discussions about his work on northern Chile. We also thank the Editor, Associate Editor, and two anonymous reviews for their helpful comments on the manuscript.

References

- Allen, T. I., & Hayes, G. P. (2017). Alternative rupture-scaling relationships for subduction interface and other offshore environments. *Bulletin of the Seismological Society of America*, 107(3), 1240–1253. <https://doi.org/10.1785/0120160255>
- Allmann, B. P., & Shearer, P. M. (2009). Global variations of stress drop for moderate to large earthquakes. *Journal of Geophysical Research*, 114(1), B01310. <https://doi.org/10.1029/2008jb005821>
- Astiz, L., Lay, T., & Kanamori, H. (1988). Large intermediate-depth earthquakes and the subduction process. *Physics of the Earth and Planetary Interiors*, 53(1–2), 80–166. [https://doi.org/10.1016/0031-9201\(88\)90138-0](https://doi.org/10.1016/0031-9201(88)90138-0)
- Baiesi, M., & Paczuski, M. (2004). Scale-free networks of earthquakes and aftershocks. *Physical Review E - Statistical Physics, Plasmas, Fluids, and Related Interdisciplinary Topics*, 69(6), 8. <https://doi.org/10.1103/physreve.69.066106>
- Bilek, S. L., & Lay, T. (2018). Subduction zone megathrust earthquakes. *Geosphere*, 14(4), 1468–1500. <https://doi.org/10.1130/ges01608.1>
- Boettcher, M. S., & Jordan, T. H. (2004). Earthquake scaling relations for mid-ocean ridge transform faults. *Journal of Geophysical Research*, 109(12), 1–21.
- Bondár, I., & Storchak, D. (2011). Improved location procedures at the International Seismological Centre. *Geophysical Journal International*, 186(3), 1220–1244. <https://doi.org/10.1111/j.1365-246x.2011.05107.x>
- Boneh, Y., Schottenfels, E., Kwong, K., van Zelst, I., Tong, X., Eimer, M., et al. (2019). Intermediate-depth earthquakes controlled by incoming plate hydration along bending-related faults. *Geophysical Research Letters*, 46(7), 3688–3697. <https://doi.org/10.1029/2018gl081585>
- Bouchon, M., Marsan, D., Durand, V., Campillo, M., Perfettini, H., Madariaga, R., & Gardonio, B. (2016). Potential slab deformation and plunge prior to the Tohoku, Iquique and Maule earthquakes. *Nature Geoscience*, 9(5), 380–383. <https://doi.org/10.1038/ngeo2701>
- Bouchon, M., Marsan, D., Jara, J., Socquet, A., Campillo, M., & Perfettini, H. (2018). Suspected deep interaction and triggering between giant earthquakes in the Chilean subduction zone. *Geophysical Research Letters*, 45(11), 5454–5460. <https://doi.org/10.1029/2018gl078350>
- Cabrera, L., Ruiz, S., Poli, P., Contreras-Reyes, E., Osses, A., & Mancini, R. (2021). Northern Chile intermediate-depth earthquakes controlled by plate hydration. *Geophysical Journal International*, 226(1), 78–90. <https://doi.org/10.1093/gji/ggaa565>
- Christensen, D. H., & Ruff, L. J. (1983). Outer-rise earthquakes and seismic coupling. *Geophysical Research Letters*, 10(8), 697–700. <https://doi.org/10.1029/gl010i008p00697>
- Chu, S. X., & Beroza, G. C. (2022). Aftershock productivity of intermediate-depth earthquakes in Japan. *Geophysical Journal International*, 230(1), 448–463. <https://doi.org/10.1093/gji/ggac024>
- Dascher-Cousineau, K., Brodsky, E. E., Lay, T., & Goebel, T. H. (2020). What controls variations in aftershock productivity? *Journal of Geophysical Research: Solid Earth*, 125(2), 1–18. <https://doi.org/10.1029/2019jb018111>
- Delbridge, B. G., Kita, S., Uchida, N., Johnson, C. W., Matsuzawa, T., & Bürgmann, R. (2017). Temporal variation of intermediate-depth earthquakes around the time of the M9.0 Tohoku-oki earthquake. *Geophysical Research Letters*, 44(8), 3580–3590. <https://doi.org/10.1002/2017gl072876>
- Di Giacomo, D., & Storchak, D. A. (2016). A scheme to set preferred magnitudes in the ISC Bulletin. *Journal of Seismology*, 20(2), 555–567. <https://doi.org/10.1007/s10950-015-9543-7>
- Dmowska, R., Rice, J. R., Lovison, L. C., & Josell, D. (1988). Stress transfer and seismic phenomena in coupled subduction zones during the earthquake cycle. *Journal of Geophysical Research*, 93(B7), 7869–7884. <https://doi.org/10.1029/jb093ib07p07869>
- Dziewoński, A. M., Chou, T.-A., & Woodhouse, J. H. (1981). Determination of earthquake source parameters from waveform data for studies of global and regional seismicity. *Journal of Geophysical Research*, 86(B4), 2825–2852. <https://doi.org/10.1029/jb086ib04p02825>
- Ekström, G., Nettles, M., & Dziewoński, A. (2012). The global CMT project 2004–2010: Centroid-moment tensors for 13,017 earthquakes. *Physics of the Earth and Planetary Interiors*, 200, 1–9. <https://doi.org/10.1016/j.pepi.2012.04.002>
- Ferrand, T. P., Hilaret, N., Incel, S., Deldicque, D., Labrousse, L., Gasc, J., et al. (2017). Dehydration-driven stress transfer triggers intermediate-depth earthquakes. *Nature Communications*, 8(May), 1–11. <https://doi.org/10.1038/ncomms15247>
- Florez, M. A., & Prieto, G. A. (2019). Controlling factors of seismicity and geometry in double seismic zones. *Geophysical Research Letters*, 46(8), 4174–4181. <https://doi.org/10.1029/2018gl081168>
- Frohlich, C. (1987). Aftershocks and temporal clustering of deep earthquakes. *Journal of Geophysical Research*, 92(B13), 13944–13956. <https://doi.org/10.1029/jb092ib13p13944>
- Frohlich, C. (1989). The nature of deep-focus earthquakes. *Annual Review of Earth and Planetary Sciences*, 17(1), 227–254. <https://doi.org/10.1146/annurev.ea.17.050189.001303>
- Gomberg, J., & Bodin, P. (2021). The productivity of Cascadia aftershock sequences. *Bulletin of the Geological Society of America*, 111(3), 1494–1507. <https://doi.org/10.1785/0120200344>
- Green, H. W., & Houston, H. (1995). The mechanics of deep earthquakes. *Annual Review of Earth and Planetary Sciences*, 23(1), 169–213. <https://doi.org/10.1146/annurev.ea.23.050195.001125>
- Hacker, B. R., Peacock, S. M., Abers, G. A., & Holloway, S. D. (2003). Subduction factory 2. Are intermediate-depth earthquakes in subducting slabs linked to metamorphic dehydration reactions? *Journal of Geophysical Research*, 108(B1). <https://doi.org/10.1029/2001jb001129>
- Hainzl, S., Brietzke, G. B., & Zöller, G. (2010). Quantitative earthquake forecasts resulting from static stress triggering. *Journal of Geophysical Research*, 115(11), 1–9. <https://doi.org/10.1029/2010jb007473>
- Hayes, G. P., Moore, G. L., Portner, D. E., Hearne, M., Flamme, H., Furtney, M., & Smoczyk, G. M. (2018). Slab2, a comprehensive subduction zone geometry model. *Science*, 362(6410), 58–61. <https://doi.org/10.1126/science.aat4723>
- Hobbs, B. E., & Ord, A. (1988). Plastic instabilities: Implications for the origin of intermediate and deep focus earthquakes. *Journal of Geophysical Research*, 93(B9), 10521–10540. <https://doi.org/10.1029/jb093ib09p10521>
- Jara, J., Socquet, A., Marsan, D., & Bouchon, M. (2017). Long-term Interactions between intermediate depth and shallow seismicity in North Chile subduction zone. *Geophysical Research Letters*, 44(18), 9283–9292. <https://doi.org/10.1002/2017gl075029>
- John, T., Medvedev, S., Rüpke, L. H., Andersen, T. B., Podladchikov, Y. Y., & Austrheim, H. (2009). Generation of intermediate-depth earthquakes by self-localizing thermal runaway. *Nature Geoscience*, 2(2), 137–140. <https://doi.org/10.1038/ngeo419>
- Kagan, Y. Y. (2003). Accuracy of modern global earthquake catalogs. *Physics of the Earth and Planetary Interiors*, 135(2–3), 173–209. [https://doi.org/10.1016/s0031-9201\(02\)00214-5](https://doi.org/10.1016/s0031-9201(02)00214-5)
- Kelemen, P. B., & Hirth, G. (2007). A periodic shear-heating mechanism for intermediate-depth earthquakes in the mantle. *Nature*, 446(7137), 787–790. <https://doi.org/10.1038/nature05717>
- King, G. C. P., Stein, R. S., & Lin, J. (1994). Static stress changes and the triggering of earthquakes. *Bulletin of the Seismological Society of America*, 84(3), 935–953.
- Lay, T., Astiz, L., Kanamori, H., & Christensen, D. H. (1989). Temporal variation of large intraplate earthquakes in coupled subduction zones. *Physics of the Earth and Planetary Interiors*, 54(3–4), 258–312. [https://doi.org/10.1016/0031-9201\(89\)90247-1](https://doi.org/10.1016/0031-9201(89)90247-1)

- Lin, J., & Stein, R. S. (2004). Stress triggering in thrust and subduction earthquakes and stress interaction between the southern San Andreas and nearby thrust and strike-slip faults. *Journal of Geophysical Research*, *109*(B2), 2303. <https://doi.org/10.1029/2003jb002607>
- Luo, Y., & Wiens, D. A. (2020). High rates of deep earthquake dynamic triggering in the thermal Halos of subducting slabs. *Geophysical Research Letters*, *47*(8), 1–10. <https://doi.org/10.1029/2019gl086125>
- Matthews, M. V., & Reasenberg, P. A. (1988). Statistical methods for investigating quiescence and other temporal seismicity patterns. *Pure and Applied Geophysics*, *126*(2–4), 357–372. <https://doi.org/10.1007/bf00879003>
- Mitsui, Y., Muramatsu, H., & Tanaka, Y. (2021). Slow deformation event between large intraslab earthquakes at the Tonga Trench. *Scientific Reports*, *11*(1), 1–8. <https://doi.org/10.1038/s41598-020-80728-w>
- Ogawa, S. (1987). Shear instability in a viscoelastic material as the cause of deep focus earthquakes. *Journal of Geophysical Research*, *92*(B13), 13801–13810. <https://doi.org/10.1029/jb092ib13p13801>
- Okada, Y. (1992). Internal deformation due to shear and tensile faults in a half-space. *Bulletin of the Seismological Society of America*, *82*(2), 1018–1040. <https://doi.org/10.1785/bssa0820021018>
- Persh, S. E., & Houston, H. (2004). Strongly depth-dependent aftershock production in deep earthquakes. *Bulletin of the Seismological Society of America*, *94*(5), 1808–1816. <https://doi.org/10.1785/012003191>
- Poli, P., & Prieto, G. A. (2016). Global rupture parameters for deep and intermediate-depth earthquakes. *Journal of Geophysical Research: Solid Earth*, *121*(12), 8871–8887. <https://doi.org/10.1002/2016jb013521>
- Ruiz, S., Metois, M., Fuenzalida, A., Ruiz, J., Leyton, F., Grandin, R., et al. (2014). Intense foreshocks and a slow slip event preceded the 2014 Iquique Mw8.1 earthquake. *Science*, *345*(6201), 1165–1169. <https://doi.org/10.1126/science.1256074>
- Sandiford, D., Moresi, L. M., Sandiford, M., Farrington, R., & Yang, T. (2020). The fingerprints of flexure in slab seismicity. *Tectonics*, *39*(8). <https://doi.org/10.1029/2019tc005894>
- Sippl, C., Schurr, B., Asch, G., & Kummerow, J. (2018). Seismicity structure of the Northern Chile forearc from >100,000 double-difference relocated hypocenters. *Journal of Geophysical Research: Solid Earth*, *123*(5), 4063–4087. <https://doi.org/10.1002/2017jb015384>
- Sippl, C., Schurr, B., John, T., & Hainzl, S. (2019). Filling the gap in a double seismic zone: Intraslab seismicity in Northern Chile. *Lithos*, *346–347*, 105155. <https://doi.org/10.1016/j.lithos.2019.105155>
- Tian, D., Wei, S. S., Wang, W., & Wang, F. (2022). Stress drops of intermediate-depth and deep earthquakes in the Tonga slab. *Journal of Geophysical Research: Solid Earth*, *127*(10). <https://doi.org/10.1029/2022jb025109>
- Tibi, R., Wiens, D. A., & Inoue, H. (2003). Remote triggering of deep earthquakes in the 2002 Tonga sequences. *Nature*, *424*(6951), 921–925. <https://doi.org/10.1038/nature01903>
- Warren, L. M., Hughes, A. N., & Silver, P. G. (2007). Earthquake mechanics and deformation in the Tonga-Kermadec subduction zone from fault plane orientations of intermediate- and deep-focus earthquakes. *Journal of Geophysical Research*, *112*(5), 1–17. <https://doi.org/10.1029/2006jb004677>
- Wei, S. S., Wiens, D. A., van Keken, P. E., & Cai, C. (2017). Slab temperature controls on the Tonga double seismic zone and slab mantle dehydration. *Science Advances*, *3*(1), 1–10.
- Wetzler, N., Brodsky, E. E., & Lay, T. (2016). Regional and stress drop effects on aftershock productivity of large megathrust earthquakes. *Geophysical Research Letters*, *43*(23), 012–12. <https://doi.org/10.1002/2016gl071104>
- Wiens, D. A., & Gilbert, H. J. (1996). Effect of slab temperature on deep-earthquake aftershock productivity and magnitude-frequency relations. *Nature*, *384*(6605), 153–156. <https://doi.org/10.1038/384153a0>
- Wimpenny, S., & Watson, C. S. (2020). gWFM: A global catalog of moderate-magnitude earthquakes studied using teleseismic body waves. *Seismological Research Letters*, *92*(1), 212–226. <https://doi.org/10.1785/0220200218>
- Ye, L., Lay, T., & Kanamori, H. (2020). Anomalous low aftershock productivity of the 2019 MW 8.0 energetic intermediate-depth faulting beneath Peru. *Earth and Planetary Science Letters*, *549*, 116528. <https://doi.org/10.1016/j.epsl.2020.116528>
- Zaliapin, I., & Ben-Zion, Y. (2013). Earthquake clusters in southern California I: Identification and stability. *Journal of Geophysical Research: Solid Earth*, *118*(6), 2847–2864. <https://doi.org/10.1002/jgrb.50179>
- Zaliapin, I., Gabrielov, A., Keilis-Borok, V., & Wong, H. (2008). Clustering analysis of seismicity and aftershock identification. *Physical Review Letters*, *101*(1), 4–7. <https://doi.org/10.1103/physrevlett.101.018501>
- Zhan, Z. (2020). Mechanisms and implications of deep earthquakes. *Annual Review of Earth and Planetary Sciences*, *48*(1), 147–174. <https://doi.org/10.1146/annurev-earth-053018-060314>
- Zhan, Z., & Shearer, P. M. (2015). Possible seasonality in large deep-focus earthquakes. *Geophysical Research Letters*, *42*(18), 7366–7373. <https://doi.org/10.1002/2015gl065088>